HOLCOMBE DEPARTMENT OF ELECTRICAL AND COMPUTER

ENGINEERING

CLEMSON UNIVERSITY

CLEMSON, SC 29634-0195

THE EFFECTS OF TRANSIENT SIGNAL PROPAGATION THROUGH ELECTRONIC SYSTEMS IN FDTD

by

Anthony Q. Martin and Chaitanya Sreerama

October 2004

for

U.S. Department of Defense

under MURI Grant F49620-01-1-0436 from the U.S. Air Force Office of Scientific Research

Report Documentation Page

Form Approved
OMB No. 0704-0188

1. REPORT DATE	2. REPORT TYPE	3. DATES COVERED
2004	**N/A**	**-**

4. TITLE AND SUBTITLE	5a. CONTRACT NUMBER
The Effects Of Transient Signal Propagation Through Electronic Systems In FDTD	5b. GRANT NUMBER
	5c. PROGRAM ELEMENT NUMBER
6. AUTHOR(S)	5d. PROJECT NUMBER
	5e. TASK NUMBER
	5f. WORK UNIT NUMBER
7. PERFORMING ORGANIZATION NAME(S) AND ADDRESS(ES) **Holcombe Department Of Electrical And Computer Engineering Clemson University Clemson, SC 29634-0195**	8. PERFORMING ORGANIZATION REPORT NUMBER
9. SPONSORING/MONITORING AGENCY NAME(S) AND ADDRESS(ES)	10. SPONSOR/MONITOR'S ACRONYM(S)
	11. SPONSOR/MONITOR'S REPORT NUMBER(S)

12. DISTRIBUTION/AVAILABILITY STATEMENT
Approved for public release, distribution unlimited

13. SUPPLEMENTARY NOTES
The original document contains color images.

14. ABSTRACT

15. SUBJECT TERMS

16. SECURITY CLASSIFICATION OF:			17. LIMITATION OF ABSTRACT	18. NUMBER OF PAGES	19a. NAME OF RESPONSIBLE PERSON
a. REPORT	b. ABSTRACT	c. THIS PAGE			
unclassified	**unclassified**	**unclassified**	**UU**	**64**	

ABSTRACT

The effects of transmission path (and environment) on the characteristics of a transient signal due to HPM sources as it passes through electronic systems are of importance in discovering how the digital circuits might be altered, since such signals are unexpected and contain spurious electromagnetic energy. Theses effects can be studied by numerically modeling the propagation of the transient signals through electronic systems such as a mock personal computer. For estimating the wideband system response most efficiently, a preliminary analysis is presented on the use of extrapolation techniques to extrapolate in both time and frequency domains simultaneously using Orthonormal associate hermite polynomials.

This page left intentionally blank.

This page left intentionally blank.

TABLE OF CONTENTS

LIST OF FIGURES

Page

CHAPTER 1
INTRODUCTION

The influence of the transmission path and environment on the characteristics of a transient signal as it passes through an electronic system is of importance in discovering how the operation of digital circuits might be altered as a result of unexpected or spurious electromagnetic energy being incident upon, and propagating through, an electronic system. If a signal of a specified form enters a system at a given point it is useful to know the salient features of the resulting signal that reaches some location within the system, where a susceptible digital circuit could be located. Moreover, it is useful to know if any of the features of the induced signal are primarily those peculiar to the entering signal, or if they are more influenced by the properties of the transmission path and/or environment. Addressing these issues should help one gain an appreciation for the nature of a spurious signal arriving at the input of a digital circuit embedded deep within a complex system and perhaps this information can be used for designing and building better high performance systems.

Firstly, the influence of the transmission path (and environment) on the shape and magnitude of a transient signal is considered by numerically modeling the signal propagation through a variety of structures that contain certain features present in the real-world systems. Structures that electromagnetically replicate only the important details of the component configurations found in typical real-world systems are considered. Examples of such systems include aircrafts, missiles, ground vehicles, personal computers, and electronic test equipment.

With the powerful Maxwell equations solvers available today to perform electromagnetic simulation it is reasonable to assume they can be useful in characterization of such effects. However, given the complexity of real-world systems this still remains a daunting task, especially when wideband characterization is needed. For example, the use of the popular FDTD method for modeling electronics inside enclosures imposes serious memory, time, and accuracy constraints in generating the late-time response. Also, the use of MOM or FEM when generating the high-frequency response can be computationally overwhelming. Recently, researchers have reported on wideband extrapolation techniques which can potentially overcome some of these limitations by using only early-time and low-frequency data. By using only the early time and low frequency data, which contain mutually complementary information, one can simultaneously extrapolate the entire system response in both domains.

Finally, we shall examine how well these extrapolation techniques work for computing the signal that penetrates an enclosure due to an exterior transient source such as a HPM source. The FDTD method will be used to obtain the early-time response and a triangular surface patch code (or some other MOM-based code) will be used to obtain the low-frequency response. Hence, the numerical models will represent different discretization of the enclosures. To further reduce complexity, only the features deemed electromagnetically essential and tractable will be included in the models. Attempts will be made to ascertain the accuracy of the approach as well as the CPU time savings measured against using either the FDTD or MOM tools separately.

CHAPTER 2
TRANSIENT SIGNAL PENETRATION INTO ELECTRONIC SYSTEMS

I. INTRODUCTION

Electromagnetic interference has become a limiting factor in digital computer performance. The effects of electromagnetic waves on highly sensitive digital circuits composed of minute circuit elements are very complex and difficult to understand. Simple mismatches, slots, or discontinuities can cause coupling in the printed circuit boards. Metal traces both with and without bends are likely to have reactive impedances that degrade the performance of complex, high-speed circuitry surrounding them. Knowledge of such electromagnetic wave effects can be very helpful for designing and building better high performance systems. Such knowledge can also be helpful in saving human lives as the need for bloodshed is reduced if enemy electronic systems can be adversely affected through proper exposure to electromagnetic interference. Likewise, human lives can be saved by designing systems harden against such threats.

The goal of this chapter is to predict the properties of a transient signal as it makes its way through a propagation path from the exterior of a structure or substrate to the terminals of a deeply embedded digital system or circuit and to catalog the properties of signals that might be expected to reach deep inside digital systems. Firstly, a widely used electronic system -- a personal computer (PC) is studied by electromagnetically replicating only the most important details of its component configuration in FDTD using

specialized procedures to model UPML, thin slots, and wire antennas as described in in the literature. The effects of the transient signal propagation through the modeled electronic system using a thin-wire antenna with a transmission line feed to excite the PC are then viewed for various time-varying waveform excitations. The concentration of the transient fields at various locations in the model is studied to access more information about the electromagnetic wave effects at those locations. Moving a step forward to further analyze the effects of the propagation path on the penetration of signals into the electronic system, a bent wire structure is modeled to electromagnetically replicate a power supply cord coming from the outside the system and terminating at the power supply unit and the disk drives. The bent wire structures terminating at the power supply unit and the CD drive are modeled very close to one another to study the effects of the propagation path and the coupling effects of closely spaced wire bundles in real PCs.

II. COMPUTATIONAL MODEL

Consider a widely used electronic system like the small, shoe-box sized Shuttle PC shown in Fig. 2-1. The Shuttle PC was considered because of its features, which resemble those of a typical desktop PC, and its compact size. The features of this PC are closely studied in order to electromagnetically replicate only the important details of the component configuration found in typical real-world PCs. The electromagnetic replica called the mock PC consists of conducting walls with slots for air vents on both sides and on the back, hollow PEC cavities for the various devices like floppy, CD, and hard drive, and the power supply unit as shown in Fig. 2-2.

(a) The front view

(b) The rear view

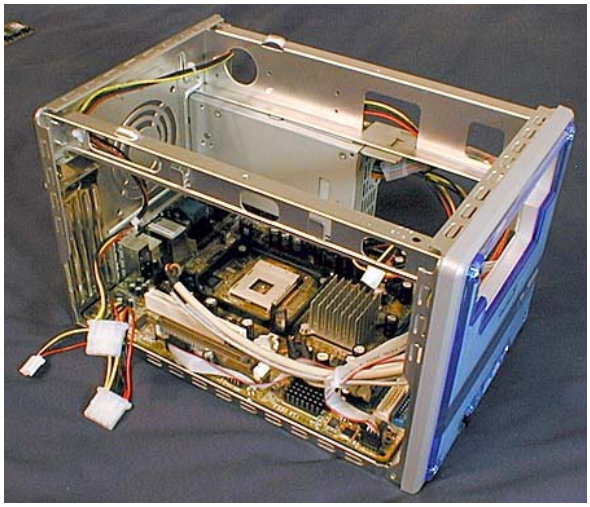

(c) The side view showing its internal structural content.

Fig. 2-1. Pictures of (a) the front view, (b) the rear view, and (c) the side view showing its internal structural content, of the Shuttle PC

The computational domain for the FDTD model of the mock PC is first terminated with PEC walls on all six sides, making it a rectangular PEC box. To simulate an open space region, UPML of thickness 15 cells is laid on the surrounding five walls.

The rectangular chassis of the mock PC, which is made of PEC, is then modeled on an infinite ground plane. The dimensions of the mock PC model shown in Fig. 2-4 are as mentioned below:

- The chassis of the mock PC is a rectangular PEC box of dimensions $30\text{cm} \times 20\text{cm} \times 20\text{cm}$, and its mesh dimensions are $60\Delta \times 40\Delta \times 40\Delta$ where $\Delta x = \Delta y = \Delta z = \Delta = 0.005$ m and $\Delta t = 0.0083$ ns.
- It consists of the following:
    - CD-ROM drive of dimension $32\Delta \times 30\Delta \times 10\Delta$
    - Floppy drive of dimension $32\Delta \times 20\Delta \times 10\Delta$
    - Hard disk of dimension $26\Delta \times 5\Delta \times 30\Delta$
    - Heat sink of dimension $15\Delta \times 15\Delta \times 10\Delta$ located 10Δ above the ground plane
    - The power supply unit of dimension $15\Delta \times 10\Delta \times 18\Delta$

  These are modeled as crude, hollow blocks of PEC
- Illuminated by a thin-wire monopole antenna of length $l = 20\Delta$ and radius $a =$ 0.003m located 15Δ from the back of the mock PC along its center line –see Fig. 2-2.
- The wire antenna is fed with a transmission line of characteristic impedance $Z_0 = 50\Omega$. An incident waveform is introduced in the transmission line using a one-way injector as described in Chapter 5.
- There are vent slots of width 0.5Δ on both sides of the mock PC to replicate the air vents in the Shuttle PC. These thin slots are modeled using the ETSF mentioned in Chapter 3.

- As indicated in Fig. 2-2 (c), the vent slots at the rear of the mock PC for the heat sink fan are of thickness Δ and all the other slots on the power supply unit are of width 0.5Δ. Here again the sub-cellular slots are modeled using the ETSF described in Chapter 4.

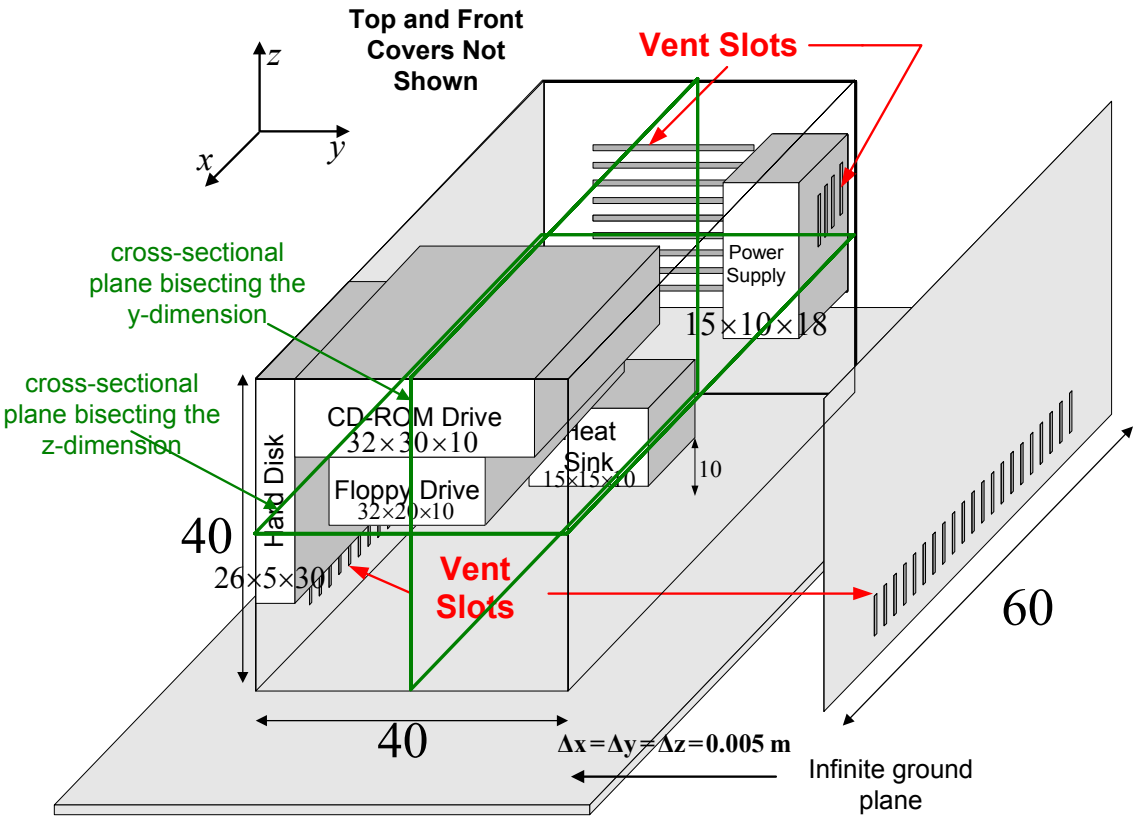

(a) The over all computational model

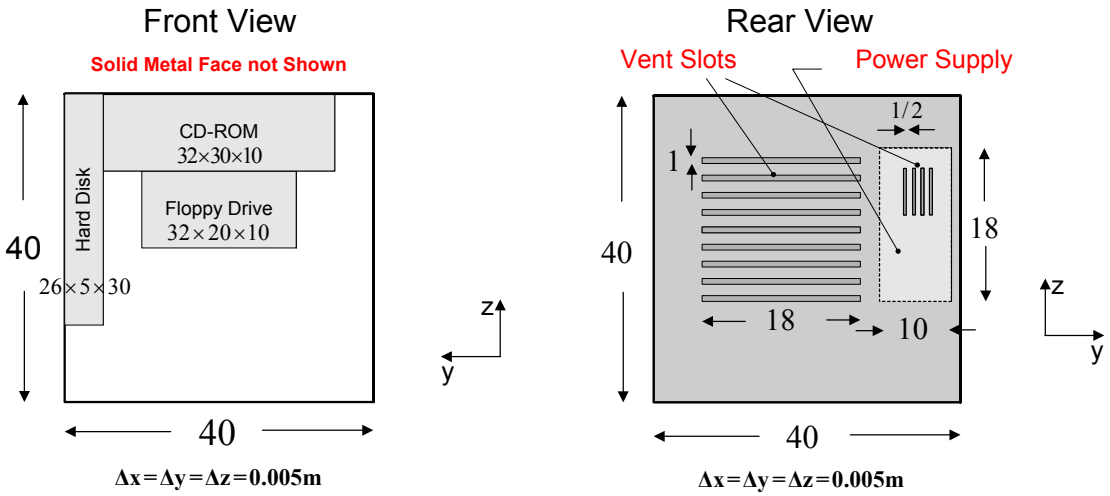

(b) The front view

(b) The rear view

Fig. 2-2. (a) The over all computational model, (b) the front view, and (c) the rear view of the mock PC

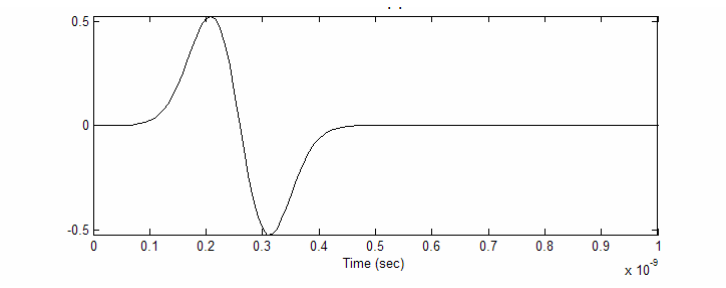

(a) The differentiated Gaussian pulse

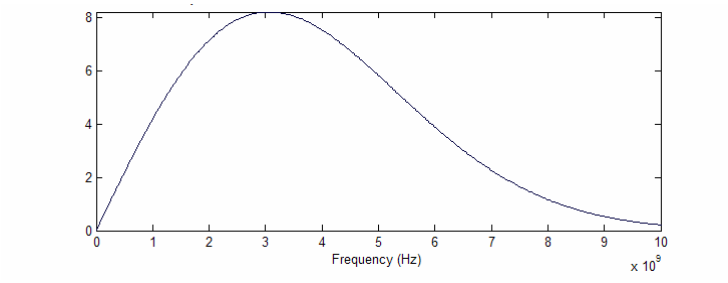

(b) The frequency spectrum of the differentiated Gaussian pulse

Fig. 2-3. (a) The differentiated Gaussian pulse and (b) the frequency spectrum of the differentiated Gaussian pulse introduced into the transmission line feed of the thin-wire antenna, used to illuminate the mock PC from behind

III. Transient Signal Penetration

In the analysis of transient signal penetration into the mock PC, the aforementioned thin-wire monopole antenna is excited at is base by the differentiated Gaussian pulse of Fig. 2-3. The cross-sectional plane bisecting the y-dimension of the mock PC in Fig. 2-2 is shown in Fig. 2-4 so that the monopole antenna may be seen.

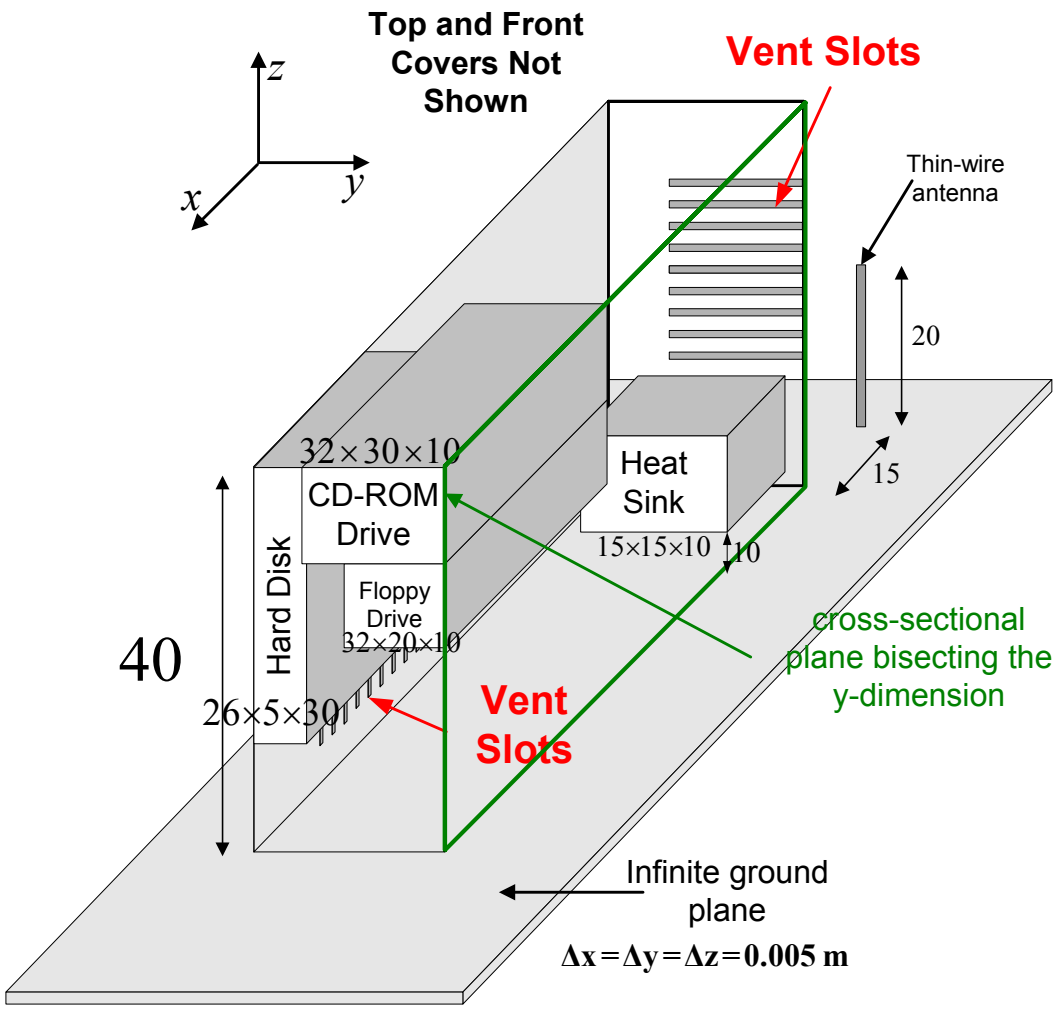

Fig. 2-4. The cross-sectional plane bisecting the y-dimension of the mock PC

Viewing the fields in the plane bisecting the y-dimension (see Fig. 2-4), one should observe zero fields inside the heat sink, the CD-ROM drive, and the floppy drive at all times, as shown in Fig. 2-5.

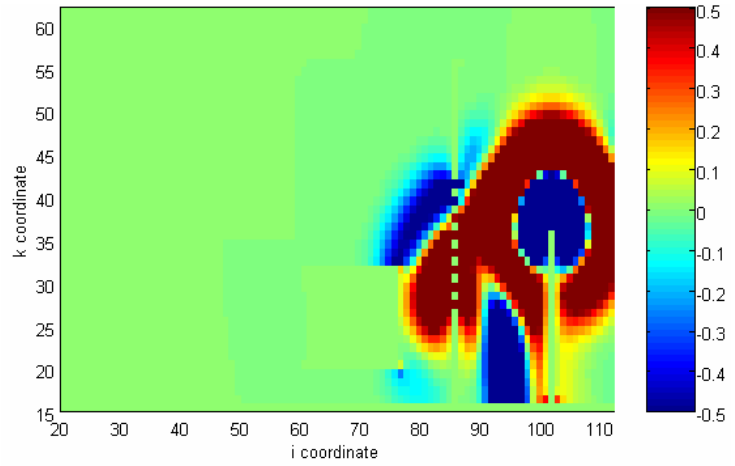

(a) Time step = 110

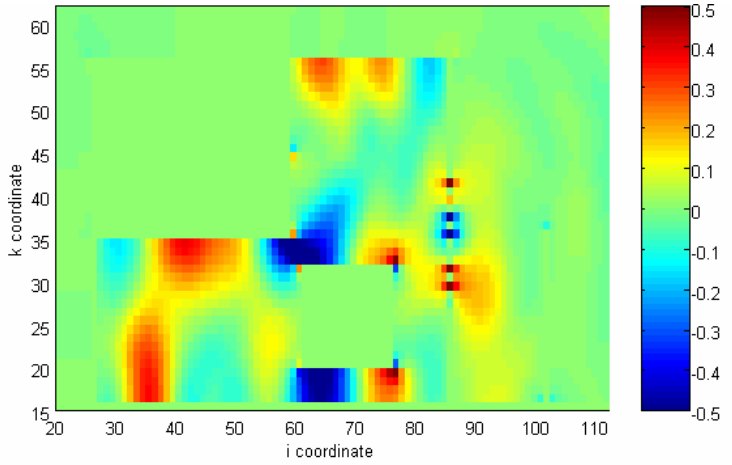

(b) Time step = 600

Fig. 2-5. The field E_z for transient signal penetration through narrow slots in the cross-sectional plane bisecting the y-dimension for (a) time step = 110 and (b) time step = 600

From Fig. 2-5 (a) at time step = 110, one can see that there is a significant amount of signal penetration into the mock PC through the vent slots in the back panel due to the near proximity of the monopole. The signals thus penetrating the system get trapped in the rectangular chassis and bounce back and forth between the PEC walls of the PC and the crude PEC models of the heat sink, CD-ROM, floppy drive, and hard drive. Fig. 2-5 (b), at time step 600, shows that the transient signals are still significant in the PC long

after the source has died. The existence of strong fields below the heat sink and near the sharp corners of the floppy drive and the heat sink might be a likely cause of electromagnetic disturbances that interrupt, obstruct, or otherwise degrade or limit the effective performance of electronics in the PC.

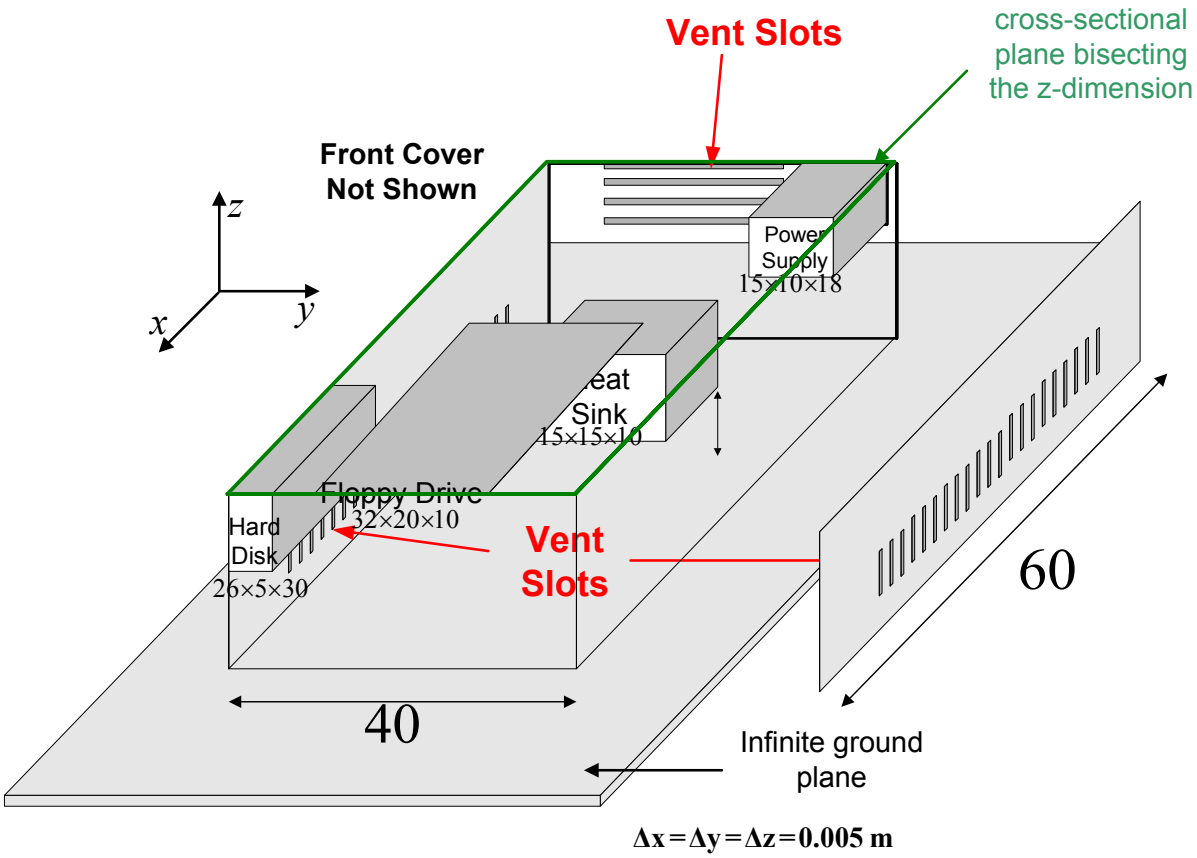

Fig. 2-6. The cross-sectional plane bisecting the z-dimension of the mock PC

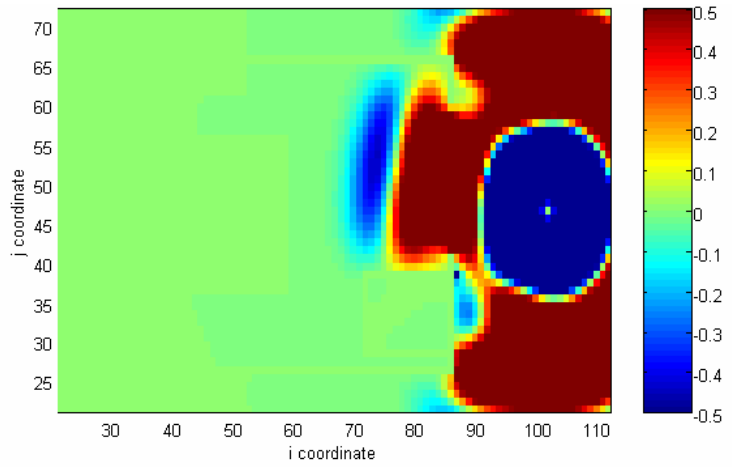

(a) Time step = 120

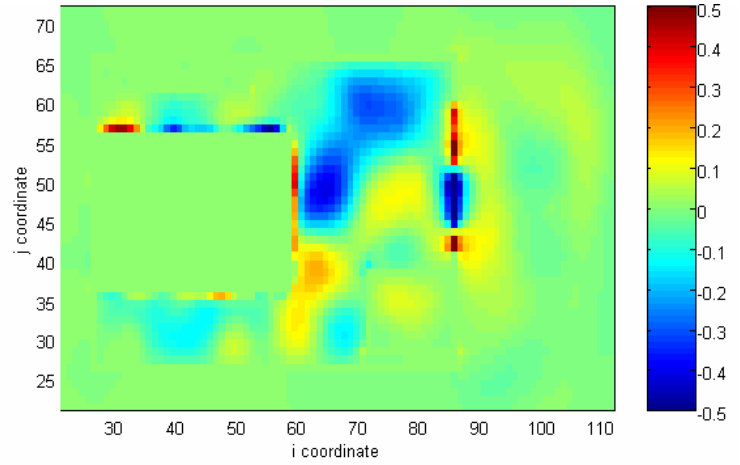

(b) Time step = 600

Fig. 2-7. The field E_z for transient signal penetration through narrow slots in the cross-sectional plane bisecting the z-dimension of the mock PC for (a) time step = 120, (b) time step = 600

Again, in the cross-sectional plane bisecting the z-dimension of the mock PC for Fig. 2-7 there are zero fields at the base of the floppy drive at all times. When there are strong fields near the monopole at time step = 120, one can see a significant amount of signal penetration into the mock PC through the vent slots in its panel nearest the monopole. When there are no fields near the monopole at time step = 600, one can see

the fields lingering inside the mock PC long after the source has died out. There is very little field penetration into the power supply unit at time step = 120 and these fields become significant as time goes on.

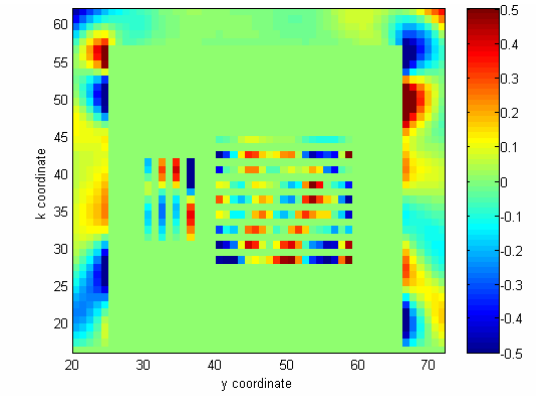

Fig. 2-8. The field E_y, which enters the mock PC from the rear panel, showing the transient signal penetration through the narrow slots at time step = 180.

To further demonstrate the significant transient signal penetration into the system through the vent slots one can view the fields penetrating the system from the slots at the rear end of the PC as shown in Fig. 2-8. Similarly, the very minor transient signal dissipation from the air vent slots located on either side of the mock PC can be viewed as shown in Fig. 2-9 (b). The field E_x, on the right hand side panel of the PC at time step = 600, also illustrates the fields lingering in the PC long after the source has died out.

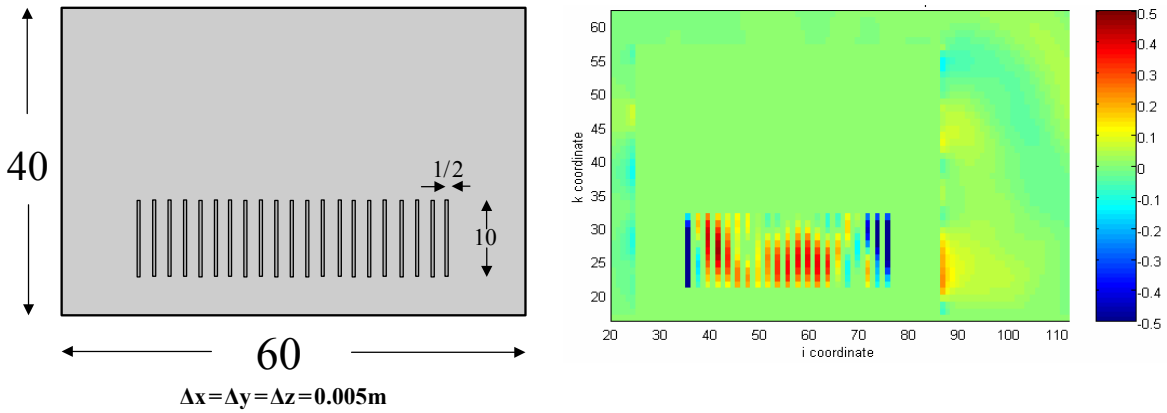

(a) (b) Time step = 600

Fig. 2-9. (a) The right hand side panel of the mock PC shown in Fig. 2-4. (b) The field E_x on the right hand side panel of the mock PC shown in (a)

To obtain a better understanding of the electromagnetic waves entering an electronic system from an outside source, the field intensities are considered at various locations in the computational model of the mock PC, as shown in Fig. 2-10. The various locations considered are the following:

- A, in the power supply unit, as waves entering this cavity section may resonate and may generate field that get transmitted to every other location in the PC that connects to the power supply unit.
- B, directly below the heat sink where the CPU and other crucial electronic circuits may be situated on the motherboard.
- C, in front of the heat sink where various electronic circuitry is located on the motherboard.
- D, behind the CD and floppy drive where the ends of the power rails from the power supply unit are found.

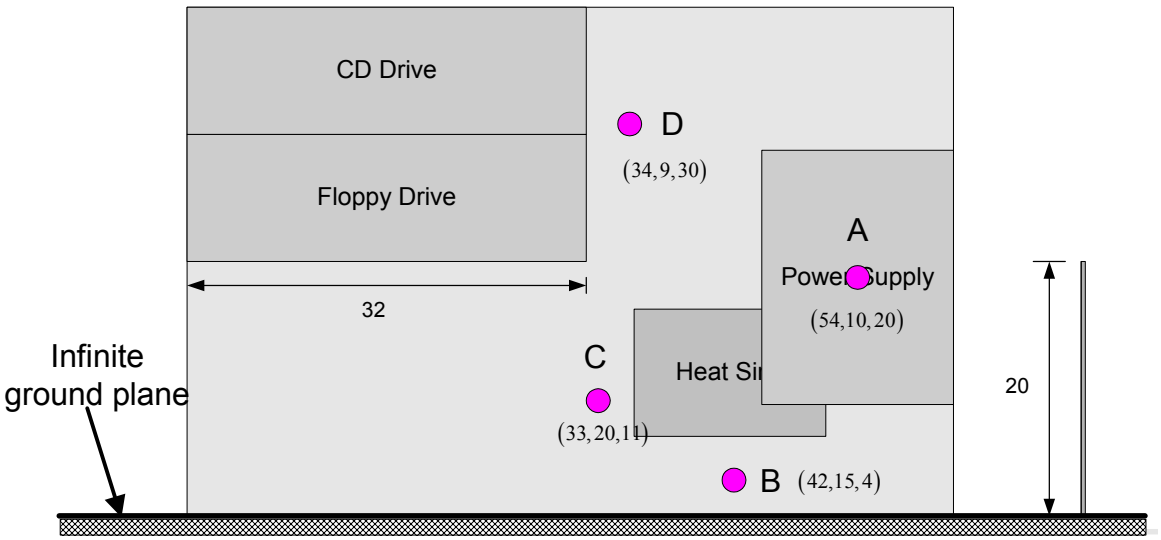

Fig. 2-10. Location of the various field points inside the mock PC

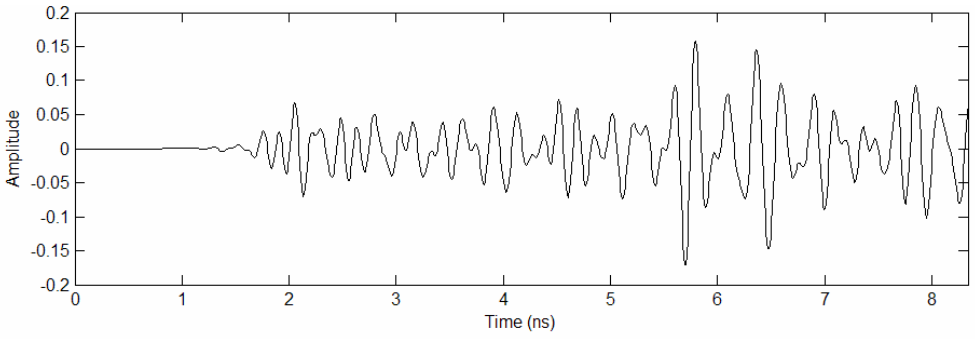

(a) the field E_z at A

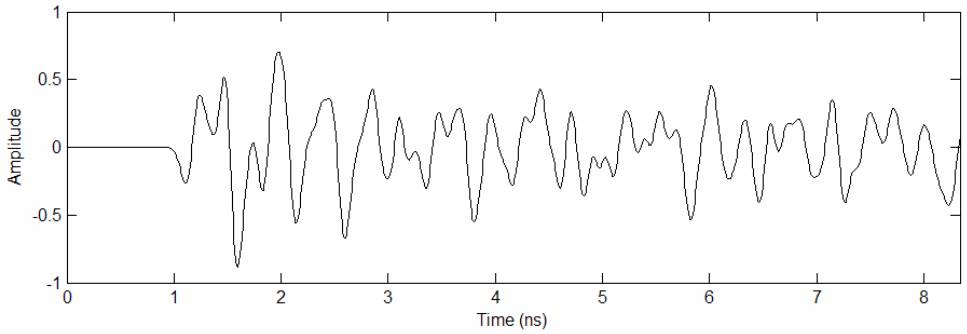

(b) the field E_z at B

Fig. 2-11. The field E_z at (a) A, (b) B, (c) C, and (d) D located in the mock PC shown in Fig. 2-10 (Continued)

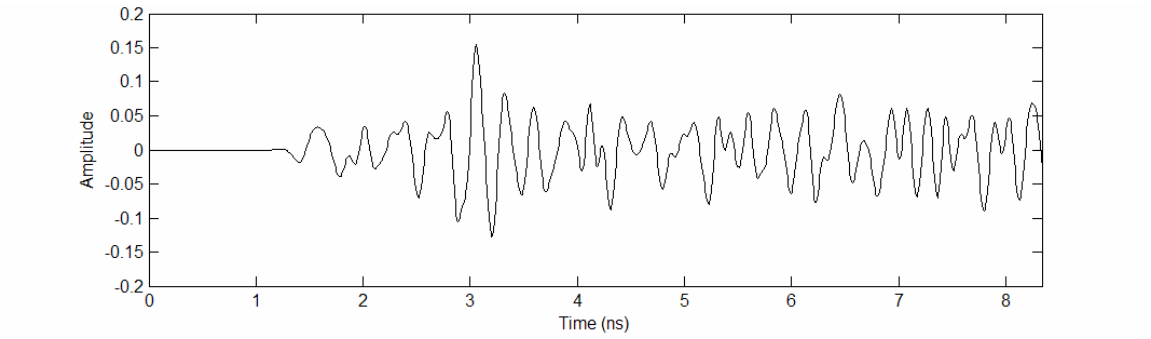

(c) the field E_z at C

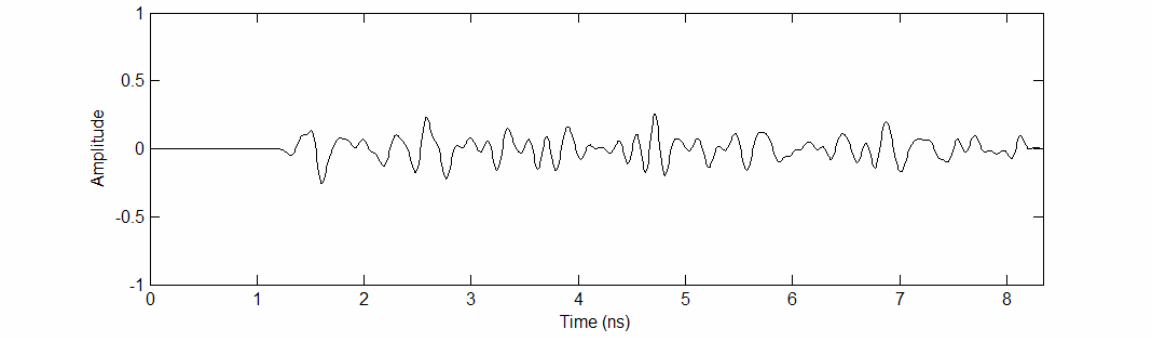

(d) the field E_z at D

Fig. 2-11. The field E_z at (a) A, (b) B, (c) C, and (d) D located in the mock PC shown in Fig. 2-10

Looking at the field E_z at the locations mentioned above, one can summarize the results shown in Fig. 2-11.

For the field E_z at point A, which is located in the power supply unit, the disturbance appears later than that at other locations. The initial amplitude of the field at this location is fairly small compared to the amplitude of the fields at other locations. The low initial amplitude indicates very little transient signal penetration into the power supply unit through the vent slots. As time passes, the fields within the power supply unit start bouncing back and forth between the walls and create a steady-state maximum

amplitude for the field, which can be attributed to the low dissipation of fields through the vent slots.

For the field at point B, located below the heat sink, there is good penetration of the fields through the slots located at the rear of the PC so a disturbance here appears much earlier and has the highest initial amplitude of all observed locations. In fact, the region below the heat sink appears to fields as a parallel plate waveguide, so the presences of strong fields is expected as is the lingering of the fields in this region long after the source has died. The existence of such high-amplitude fields where the CPU and other crucial electronic circuits may be situated on the motherboard may result in degradation of their performance.

For location C, in front of the heat sink, the amplitude of the field overall is fairly small as the heat sink acts as a barrier for the fields penetrating from the slots located directly behind. The field initially has small amplitude as the heat sink obstructs the penetrating transients from reaching the location of the field point and then increase to a maximum value, which can be attributed to the good penetration of the fields through the slots in the rear of the PC. The field then reaches a minimum after the source dies out. Finally, the field increases again due to the effect of fields lingering in the PC long after the source has died.

The amplitude of the field E_z at D, behind the CD and floppy drive, is small compared to the field at B. The field has high initial amplitude owing to good penetration of the transients thought the vent slots and decreases gradually to the amplitude of the fields lingering in the rectangular chassis of the mock PC.

IV. EFFECTS OF THE PROPAGATION PATH ON SIGNAL PENETRATION

To further analyze the effects of the propagation path on the penetration of signals into an electronic system, a bent wire is included in the mock PC, as shown in Fig. 2-12, to simulate a power supply cord coming from outside into the system. The thin wire of radius a = 0.003m emerges from the ground plane at a distance 5Δ away from the rear of the PC and rises to a height of 5Δ from the ground plane. The wire then bends and enters the PC through a square hole $3\Delta \times 3\Delta$ in size and then splits into two wires, one of which goes to the power supply unit while the other goes to a disc drive, as shown in Fig. 2-12. The two wires after the split in the bent wire are made to run very close to each other, as shown in Fig. 2-12, to see any significant effects due to propagation path and the coupling effect between closely spaced wire bundles in a real PC. The numerical procedure employed in modeling the bent-wire structure is described in detail in Chapter 4. The structure shown in Fig. 2-12 is illuminated with a thin-wire monopole of height $l = 20\Delta$ and radius a = 0.003m, placed 15Δ directly behind the PC on its centerline. The monopole is fed with a transmission line of characteristic impedance $Z_0 = 50\Omega$ and is excited with the differentiated Gaussian pulse shown in Fig. 2-3.

To view the effects of the propagation path (bent-wire structure) on the transient signal penetration into the electronic system, consider the planes along the y–dimension and the z-dimension in the cross-section including the wire, as shown in Fig. 2-13. With the structure being illuminated by the monopole, one should expect to see the transient signal penetration increase as the fields from outside get coupled to the bent wire structure leading into the PC. Indeed, while the wire structure enhances the ability of a signal to reach the interior of the PC due to conductive coupling, it also makes it possible

for trapped fields lingering inside the PC to escape into the exterior region, which shows up at later time steps in the FDTD simulation.

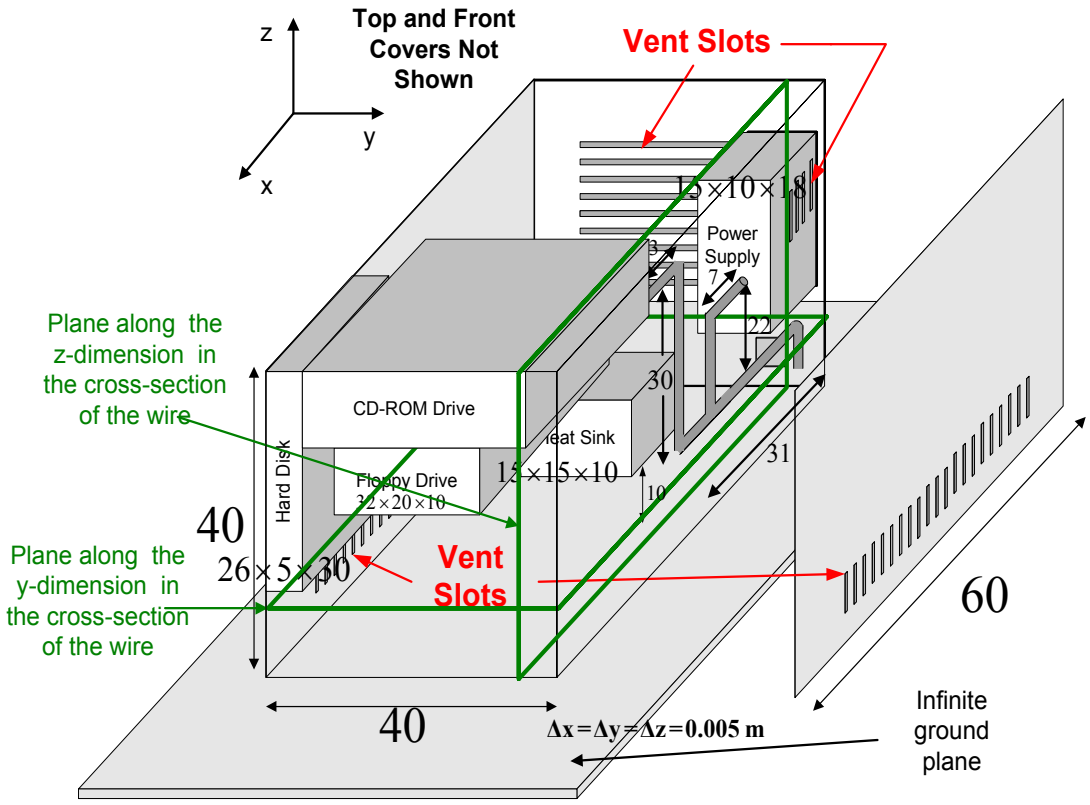

Fig. 2-12. The computational model of the mock PC with the bent-wire structure to simulate a power supply cord

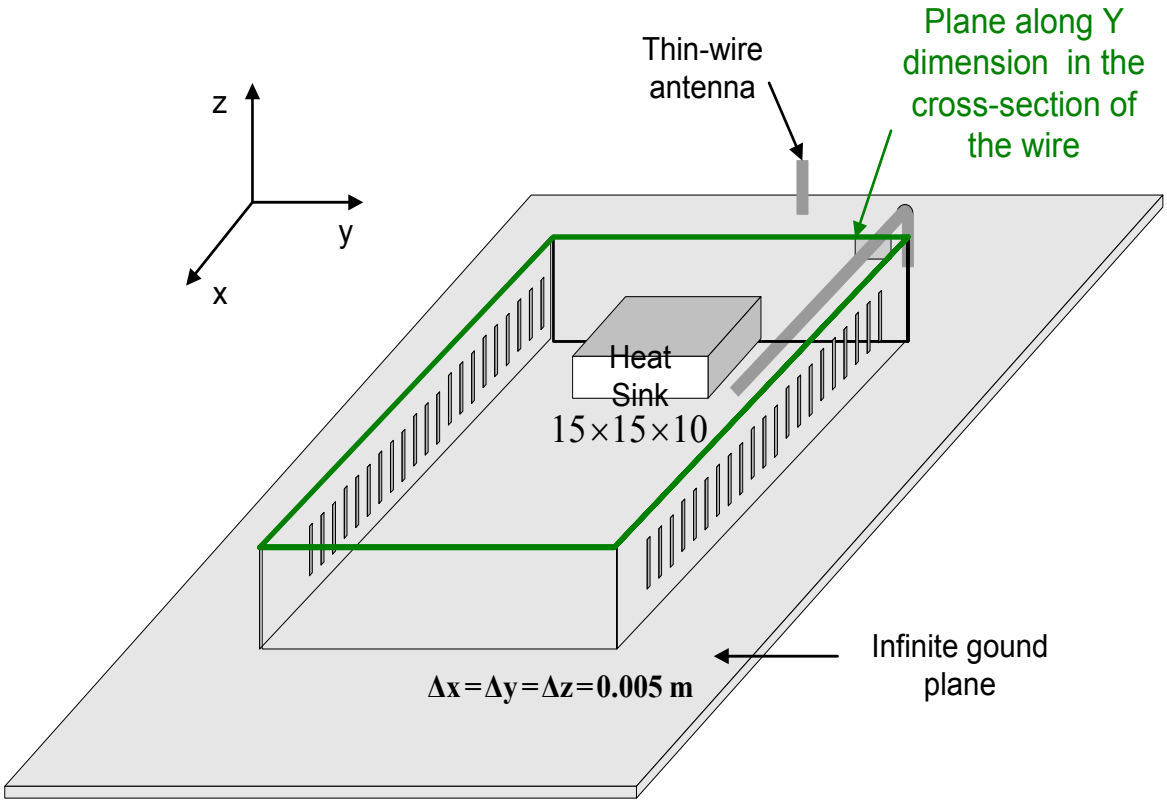

Fig. 2-13. The plane along the y-direction in the cross-section of the wire of the mock PC with the bent-wire structure

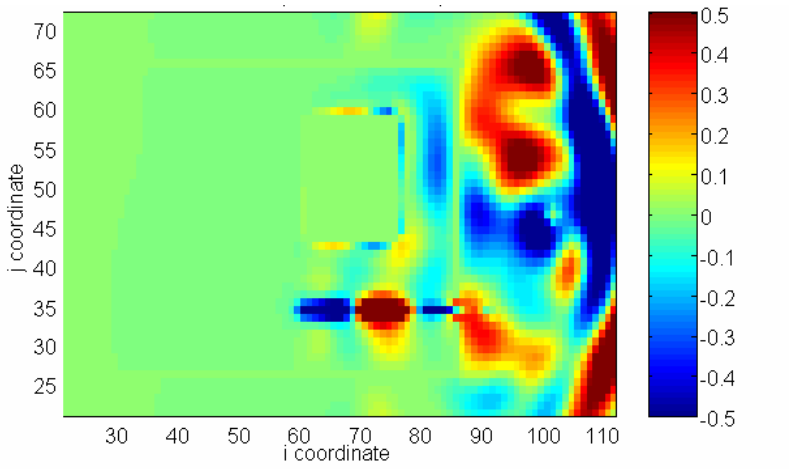

(a) Time step = 140

Fig. 2-14. The field E_z in the plane along the y-dimension in the cross-section of the wire shown in Fig. 2-13 for (a) time step = 140 and (b) time step = 1000 (Continued)

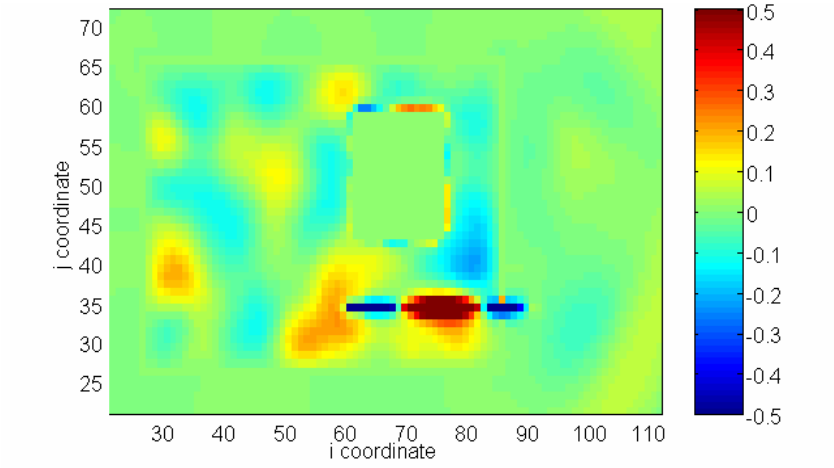

(b) time step = 1000

Fig. 2-14. The field E_z in the plane along the y-dimension in the cross-section of the wire shown in Fig. 2-13 for (a) time step = 140 and (b) time step = 1000

When the antenna initially illuminates the mock PC with the bent-wire structure, fields couple to the bent wire and make their way into the PC, as shown in the plot in Fig. 2-14 (a). In Fig. 2-14 (b) at time step = 1000, which is long after the source outside has died out, one can still see the fields lingering in the rectangular chassis of the PC, but the bent-wire structure clearly aids in dissipating the fields by enhancing radiation out the rear of the PC.

Now consider the plane along the z-dimension in the cross-section of the wire as shown in Fig. 2-15.

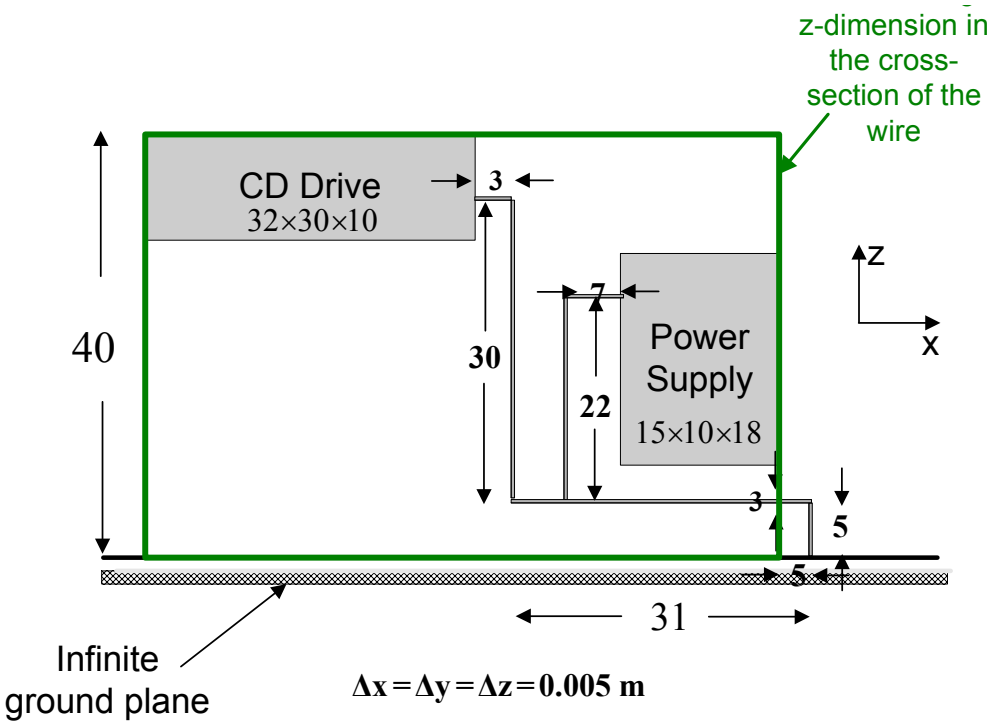

Fig. 2-15. The plane along z-dimension in the cross-section of the wire of the mock PC with the bent wire structure

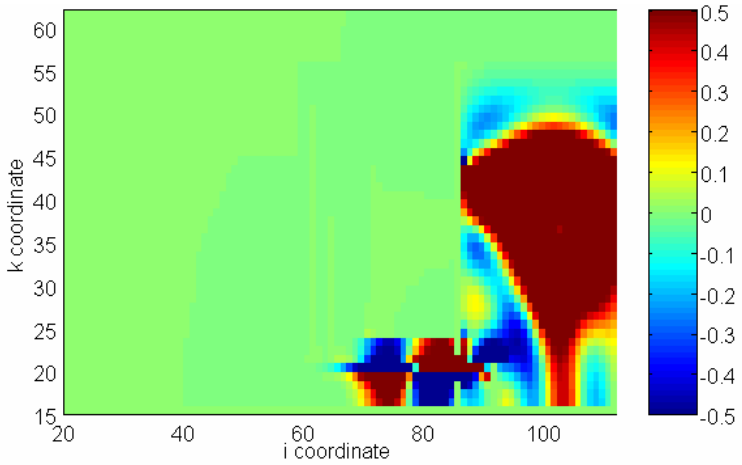

(a) Time step =120

Fig. 2-16. The field E_z in the plane along the z-dimension in the cross section of the wire shown in Fig. 2-15 for (a) time step = 120 and (b) time step = 600 (Continued)

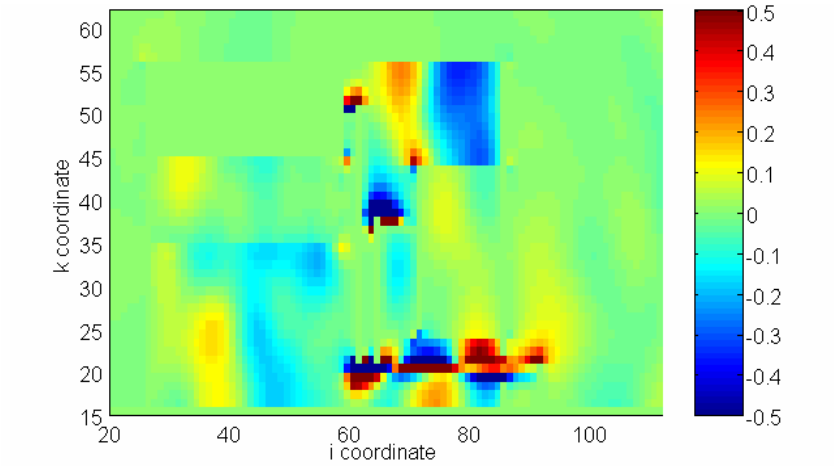

(b) Time step =600

Fig. 2-16. The field E_z in the plane along the z-dimension in the cross section of the wire shown in Fig. 2-15 for (a) time step = 120 and (b) time step = 600

The plots of the field E_z for time step = 120 in Fig. 2-16 (a) illustrates the coupling of the spurious electromagnetic energy to the wire leading into the PC. From Fig. 2-16 (b) one can see the fields still lingering in the PC long after the source outside has died and also the dissipation of the fields brought about by the bent wire. Thus, cables running into the electronic system can cause electromagnetic interference that affects the operation of digital circuits embedded deep within the system. Again, to obtain a better understanding of the electromagnetic waves entering an electronic system from an outside source, one can consider the field intensities at various locations in the computational model of the mock PC shown in Fig. 2-17.

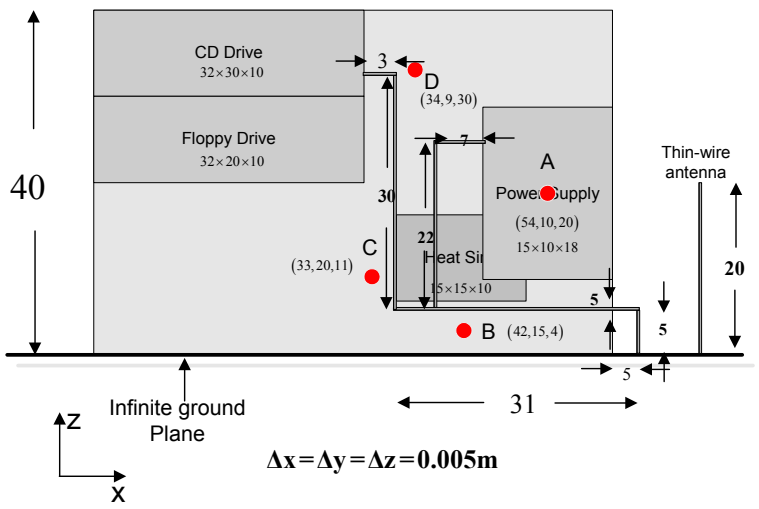

Fig. 2-17. Location of the various field points inside the mock PC with the bent-wire structure

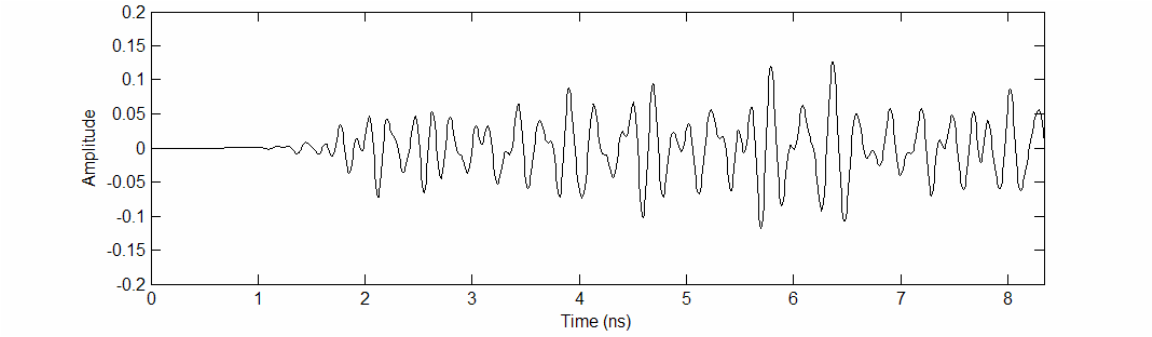

(a) the field E_z at A

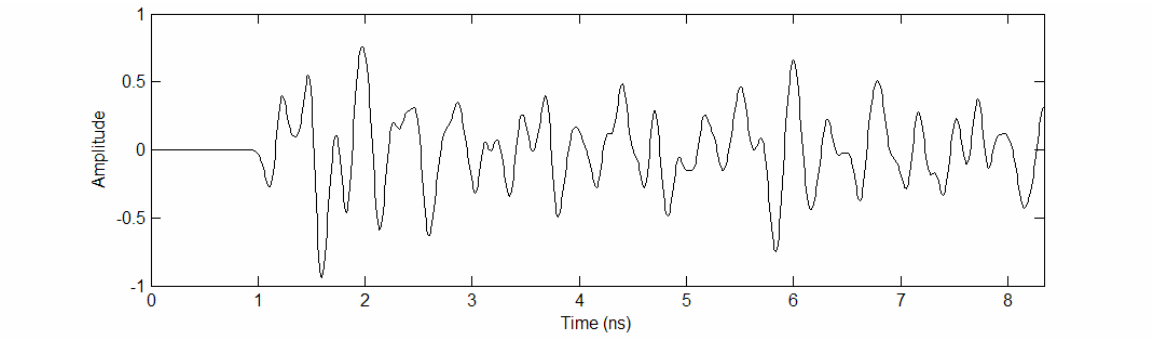

(b) the field E_z at B

Fig. 2-18. The field E_z at (a) A, (b) B, (c) C, and (d) D located in the mock PC with the bent-wire structure shown in Fig. 2-17 (Continued)

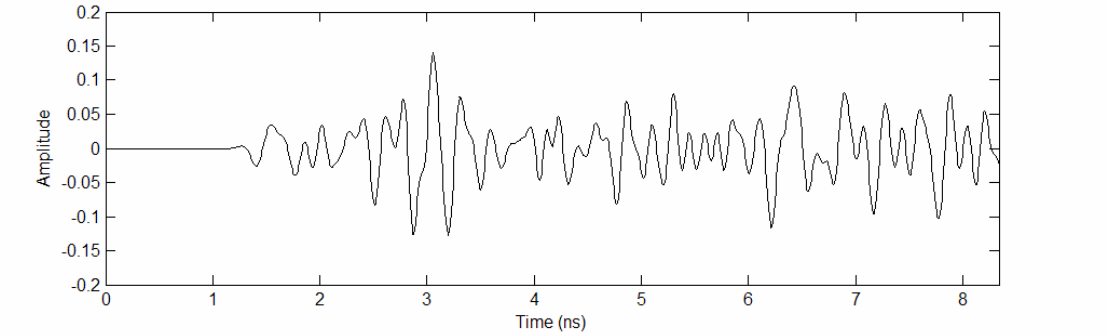

(c) the field E_z at C

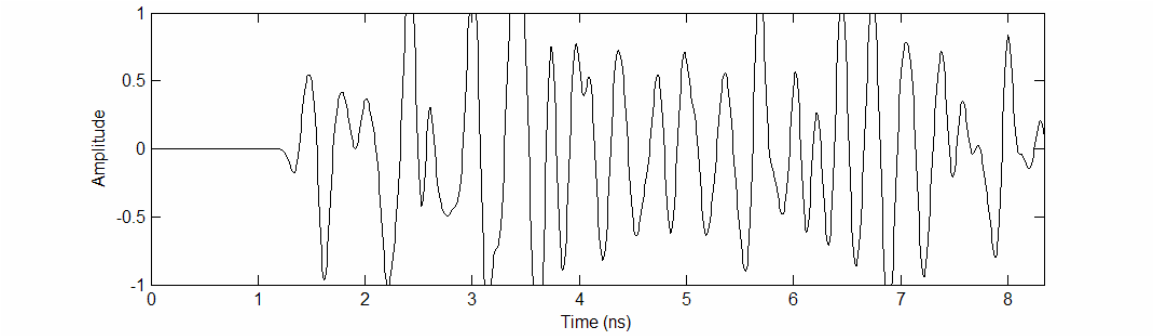

(d) the field E_z at D

Fig. 2-18. The field E_z at (a) A, (b) B, (c) C, and (d) D located in the mock PC with the bent-wire structure shown in Fig. 2-17

Comparing the field E_z at various locations in Fig. 2-10 for the cases without the bent-wire structure, as in Fig. 2-11, and with the bent-wire structure, as in Fig. 2-18, one can summarize the results in Fig. 2-18 as follows.

For point A in the power supply unit the field at this location enters at approximately the same time as the fields in other locations as the transient fields now get coupled to the wire and enter the PC. The initial amplitude of the field is fairly small but higher than the results of Fig. 2-11 (a). Again, as time passes the penetrated fields start bouncing back and forth between the walls of the power supply unit. This is observed much earlier than in the results for the model without the bent wire, which are shown in

Fig. 2-11 (a). The amplitude of the field at this location gradually decreases for late time, and this can be attributed to carrying off of energy from the unit via the bent-wire structure.

Point B is below the heat sink so the field coupling to the bent-wire structure leading results in a field with higher amplitude than that of field E_z in Fig. 2-11 (b). Due to the lingering of the fields inside the chassis of the PC long after the source has died out and the wire structure field coupling effect, the field at this location remains fairly high even for late time.

In front of the heat sink, at point C, the penetrated transient signal is very similar to Fig. 2-11 (c) with the slightly higher amplitude attributed to enhanced coupling due to the bent-wire structure.

Behind the CD and floppy drive at D the field has very high amplitude when compared to Fig. 2-11 (d), thus showing the effects of propagation path on the penetration of signals into the electronic system. The field remains high for long periods of after the source has died out due to the coupling of fields between the closely spaced wires leading to the power supply unit and the CD drive and the field scattering around the sharp bends.

V. SUMMARY

This chapter presents an overview of electromagnetic interference effects relating to the performance of an electronic system. The effects of transient electromagnetic waves on highly sensitive digital circuits in electronic systems are very complex and difficult to understand as simple mismatches, slots, or discontinuities can cause coupling in the inlaid circuits. The results presented for an electromagnetically replicated PC

model helps one to predict the properties of transient signals as they make their way through a propagation path from the exterior of a structure to the terminals of a deeply embedded digital system or circuit and to catalog the properties of signals that might be expected to reach various locations in the electronic system. Observing the dominant field component at certain specific locations in the mock PC gives one a better understanding of the behavioral patterns of the penetrating fields at these locations. Metal wires both with and without bends are likely to have reactive impedances that degrade the performance of complex, high-speed circuitry surrounding them. The model of the mock PC with the bent-wire structure showed the effects of the wires in the electronic systems. The most significant feature observed in the case of adding the bent-wire structure is the enhancement of transient signal penetration into the system, attributed to the fields getting coupled to the wire from outside. These effects of transient signal penetration into electronic systems can be further studied by adding more realistic detail to determine the causes and effects of specific components of interest and by considering other structures and excitations (pulses, pulse trains, etc.).

CHAPTER 3
EXTRAPOLATION IN TIME AND FREQUENCY DOMAINS USING ORTHONORMAL ASSOCIATE HERMITE FUNCTIONS

I. INTRODUCTION

The effects of the transmission path and environment on the characteristics of a transient signal due to a high-power microwave (HPM) source as it passes through an electronic system is of importance in discovering how the operation of digital circuits might be altered, since such signals are unexpected and contain spurious electromagnetic energy. If a signal of a specified form enters a system at a given point it is useful to know the salient features of the resulting signal that reaches a location within the system where a susceptible digital circuit is located. Moreover, it is useful to know which features of the induced signal are primarily those peculiar to the entering signal and which features are more influenced by the properties of the transmission environment. Addressing these issues should help one gain an appreciation for the nature of a spurious signal arriving at the input of a digital circuit embedded deep within a complex system, and perhaps that information can be used to eliminate deleterious effects on the operation of digital circuits.

With the powerful Maxwell equations solvers available today to perform electromagnetic simulation, it is reasonable to assume that they can be useful to

characterize such effects. However, given the complexity of real-world systems this still remains a daunting task, especially when wideband characterization is needed. For example, the use of the popular FDTD method for modeling electronics inside enclosures imposes serious memory, time, and accuracy constraints in generating the late-time response. Also, the use of MOM or FEM when generating the high-frequency response can be computationally overwhelming. Recently, researchers have developed wideband extrapolation techniques that are often capable of overcoming some of these limitations by using only early-time and low-frequency data [1]. By using only the early time and low frequency data, which contain mutually complementary information, one can simultaneously extrapolate the entire system response in both domains [2].

The focus of this chapter is to examine how well these extrapolation techniques work. The FDTD method is used to obtain the early-time response, and a MOM-based (any frequency domain MOM or FEM code could be used) is used to obtain the low-frequency response. Attempts are made to ascertain the accuracy of the approach as well as the CPU time savings measured against using either the FDTD or MOM tools separately.

II. Orthonormal Associate Hermite Functions

Using only the early time and low frequency data, which contain mutually complementary information, one can simultaneously extrapolate the entire system response in both domains using the orthonormal associate hermite (AH) functions. The isomorphism between an AH function and its Fourier transform allows one to work in both time and frequency domains simultaneously [1-3].

The associate hermite functions $h_n(x)$ are defined through hermite polynomials $H_n(x)$ as

$$h_n(x) = \frac{H_n(x)e^{\frac{-x^2}{2}}}{\left(2^n n!\sqrt{\pi}\right)^{\frac{1}{2}}} \tag{8.1}$$

where *n* is order of the hermite polynomials. The hermite polynomials are recursively expressed as

$$\begin{aligned} &H_0(x) = 1 \\ &H_1(x) = 2x \\ &H_n(x) = 2xH_{n-1}(x) - 2(n-1)H_{n-2}(x), \qquad \text{for } n \geq 2 \end{aligned} \tag{8.2}$$

using (8.2) the AH functions can be expressed as

$$\begin{aligned} h_0(x) &= \frac{e^{\frac{-x^2}{2}}}{\left(\sqrt{\pi}\right)^{\frac{1}{2}}} \\ h_1(x) &= \frac{2xe^{\frac{-x^2}{2}}}{\left(2\sqrt{\pi}\right)^{\frac{1}{2}}} \\ h_n(x) &= \frac{1}{\sqrt{n}}\left[\sqrt{2}xh_{n-1}(x) - \sqrt{n-1}h_{n-2}(x)\right], \qquad \text{for } n \geq 2 \end{aligned} \tag{8.3}$$

The plot of AH functions for orders zero to four are as shown in Fig. 3-1. The AH functions are also known as orthonormal AH functions because their polynomials are mutually orthogonal and form a complete set in the interval $[-\infty, +\infty]$ [2], given as

$$\int_{-\infty}^{\infty} h_i(x) h_j(x) dx = \delta_{ij} \tag{8.4}$$

where δ_{ij} is the Kronecker delta for which

$$\begin{aligned} \delta_{ij} &= 1, \qquad \text{for } i = j \\ \delta_{ij} &= 0, \qquad \text{otherwise} \end{aligned} \tag{8.5}$$

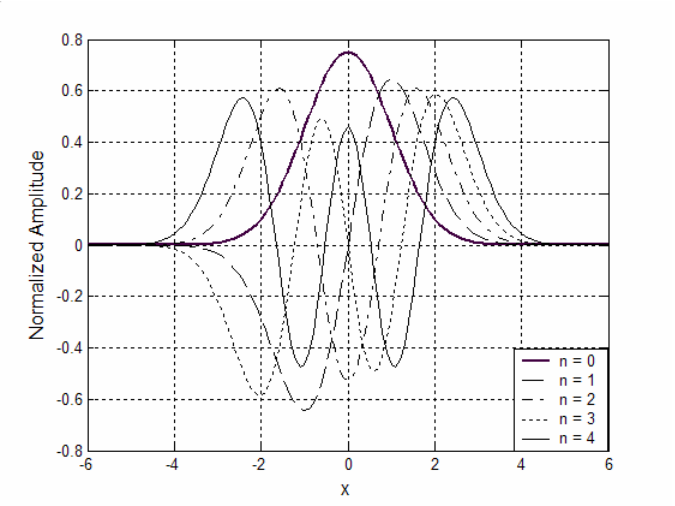

Fig. 3-1 Associate hermite functions of orders zero to four

As shown in Fig. 3-1, the AH polynomials of even order are even functions while those of odd order are odd functions

$$\begin{aligned} h_{2m}(x) &= h_{2m}(-x) \\ h_{2m+1}(x) &= -h_{2m+1}(-x) \end{aligned} \tag{8.6}$$

for any value of m. Finally, if $f(x)$ is a finite interval piecewise smooth function in the interval $[-k, k]$ and

$$\int_{-\infty}^{\infty} e^{-x^2} f^2(x)\,dx < \infty \tag{8.7}$$

then $f(x)$ can be represented as

$$f(x) = \sum_{n=0}^{\infty} a_n h_n(x), \qquad \text{for } -\infty < x < \infty \tag{8.8}$$

with

$$a_n = \int_{-\infty}^{\infty} f(x) h_n(x)\,dx \tag{8.9}$$

This series exhibits pointwise convergence to $f(x)$ wherever $f(x)$ is continuous and to $\left[f\left(x^+\right) + f\left(x^-\right)\right] \Big/ 2$ at points of discontinuity. From the property of isomorphism, the AH functions are eigenfunctions of the Fourier transform operator. To clarify, if $H_n(X)$ is defined to be the Fourier transform of $h_n(x)$ then

$$H_n(X) = \int_{-\infty}^{\infty} h_n(x) \exp(-j2\pi Xx)\,dx = (-j)^n h_n(X) \tag{8.10}$$

where $j = \sqrt{-1}$. Hence, if $F(X)$ is considered to be the Fourier transform of $f(x)$, then one can write

$$F(X) = \int_{-\infty}^{\infty} f(x) \exp(-j2\pi Xx) \tag{8.11}$$

Substituting (8.8) into (8.11)

$$F(X) = \int_{-\infty}^{\infty} \sum_n a_n h_n(x) \exp(-j2\pi Xx)\, dx \tag{8.12}$$

and hence from (8.10)

$$F(X) = \sum_n a_n (-j)^n h_n(X) \tag{8.13}$$

From (8.8) and (8.13), one can conclude that the same hermite functional representation can be used to approximate both time-domain and frequency-domain electromagnetic responses.

III. THE MATHEMATICAL FORMULATION

Let $f(t)$ be the time domain electromagnetic response due to an incident stimulus $f_{inc}(t)$. Using the orthonormal AH functions, one can represent the time-domain electromagnetic response as

$$f(t) = \sum_{n=0}^{N} \frac{a_n}{\sqrt{s_1}} h_n\left(t/\sqrt{s_1}\right) \tag{8.14}$$

where s_1 is a scaling factor for the time variable. As in (8.8), the time-domain response obtained using the time-domain techniques cannot go to infinity but only up to some value N_t because one is only interested in the obtaining the early-time response. Similarly, the frequency-domain response can also be represented in terms of AH functions. From (8.13) the frequency-domain response $F(f)$ can be written as

$$F(f) = \int_{-\infty}^{\infty} f(t) \exp(-j2\pi ft)\, dt \tag{8.15}$$

Again, as the frequency-domain response computed is finite with N_f points. Equation (8.15) can further be expressed as

$$F(f) = \sum_{n=0}^{N} (-j)^n \frac{a_n}{\sqrt{s_2}} h_n(f/s_2) \tag{8.16}$$

$$F(f) = \sum_{n=0}^{N/2} (-1)^n \left[\frac{a_{2n}}{\sqrt{s_2}} h_{2n}(f/s_2) - j \frac{a_{2n+1}}{\sqrt{s_2}} h_{2n+1}(f/s_2) \right] \tag{8.17}$$

$$F(f) = F_R(f) + jF_I(f) \tag{8.18}$$

Again s_2 is the scale factor for frequency. The scale factors in either domain are related as

$$s_2 = \frac{1}{(2\pi s_1)} \tag{8.19}$$

This extrapolation technique is most effective when the causal time domain signal $f(t)$, to be expanded in terms of AH functions, is centered about $t = t_c$, where t_c is around half the time support of $f(t)$ [1-2] because the AH functions provide equal support on either side. Centering the expansion would require fewer terms, hence the corresponding transform in the frequency domain is given as

$$f(t + t_0) = F(f) \exp(j2\pi ft_0) \tag{8.20}$$

The scaling factors are crucial because they determine the amount of support provided by the AH functions to the time and frequency domain. Using sufficient amounts of low-frequency and early time-domain data, a properly chosen order of expansion *N*, and well chosen scale factors s_1 and s_2, one can obtain the missing data (i.e., the high-frequency and late time-domain data). The order of expansion *N* is obtained by trial and error, by using a large value initially and choosing a cutoff for the magnitude of the coefficients and discarding the ones that die out. An important point to be considered while choosing the order is that an unnecessarily large *N* introduces oscillations in the results.

IV. MATRIX FORMULATION

The matrix representation of the early time-domain data in terms of the hermite functions (8.14) is expressed as

$$\begin{bmatrix} h_0(t_1/s_1) & h_1(t_1/s_1) & \cdots & h_{N-1}(t_1/s_1) \\ h_0(t_2/s_1) & h_1(t_2/s_1) & \cdots & h_{N-1}(t_2/s_1) \\ \vdots & \vdots & \vdots & \vdots \\ h_0(t_{N_t}/s_1) & h_1(t_{N_t}/s_1) & \cdots & h_{N-1}(t_{N_t}/s_1) \end{bmatrix}_{N_t \times N} \cdot \begin{bmatrix} a_0 \\ a_1 \\ \vdots \\ a_{N-1} \end{bmatrix}_{N \times 1} = \sqrt{s_1} \begin{bmatrix} f(t_1) \\ f(t_2) \\ \vdots \\ f(t_{N_t}) \end{bmatrix}_{N_t \times 1} \tag{8.21}$$

The real part of the low frequency data $F(f)$ from (8.16) can be represented in matrix form as

$$\begin{bmatrix} h_0(f_1/s_2) & -h_2(f_1/s_2) & \cdots & (-1)^{\frac{N}{2}-1} h_{N-1}(f_1/s_2) \\ h_0(f_2/s_2) & -h_2(f_2/s_2) & \cdots & (-1)^{\frac{N}{2}-1} h_{N-1}(f_2/s_2) \\ \vdots & \vdots & \vdots & \vdots \\ h_0\left(f_{N_f}/s_2\right) & -h_2\left(f_{N_f}/s_2\right) & \cdots & (-1)^{\frac{N}{2}-1} h_{N-1}\left(f_{N_f}/s_2\right) \end{bmatrix}_{N_f \times \frac{N}{2}} \cdot \begin{bmatrix} a_0 \\ a_2 \\ \vdots \\ a_{N-2} \end{bmatrix}_{\frac{N}{2}\times 1} = \sqrt{s_2} \begin{bmatrix} F_R(f_1) \\ F_R(f_2) \\ \vdots \\ F_R\left(f_{N_f}\right) \end{bmatrix}_{N_f \times 1} \tag{8.22}$$

Similarly, the imaginary part of the low frequency data $F(f)$ from (8.18) is

$$\begin{bmatrix} -h_1(f_1/s_2) & h_3(f_1/s_2) & \cdots & (-1)^{\frac{N}{2}} h_{N-2}(f_1/s_2) \\ -h_1(f_2/s_2) & h_3(f_2/s_2) & \cdots & (-1)^{\frac{N}{2}} h_{N-2}(f_2/s_2) \\ \vdots & \vdots & \vdots & \vdots \\ -h_1\left(f_{N_f}/s_2\right) & h_3\left(f_{N_f}/s_2\right) & \cdots & (-1)^{\frac{N}{2}} h_{N-2}\left(f_{N_f}/s_2\right) \end{bmatrix}_{N_f \times \frac{N}{2}} \cdot \begin{bmatrix} a_1 \\ a_3 \\ \vdots \\ a_{N-1} \end{bmatrix}_{\frac{N}{2}\times 1} = \sqrt{s_2} \begin{bmatrix} F_I(f_1) \\ F_I(f_2) \\ \vdots \\ F_I\left(f_{N_f}\right) \end{bmatrix}_{N_f \times 1} \tag{8.23}$$

Combining (8.21), (8.22), and (8.23),

$$\begin{bmatrix} h_0(t_1/s_1) & h_1(t_1/s_1) & \cdots & h_{N-1}(t_1/s_1) \\ \vdots & \vdots & \vdots & \vdots \\ h_0(t_{N_t}/s_1) & h_1(t_{N_t}/s_1) & \cdots & h_{N-1}(t_{N_t}/s_1) \\ h_0(f_1/s_2) & -h_2(f_1/s_2) & \cdots & (-1)^{\frac{N}{2}-1} h_{N-1}(f_1/s_2) \\ \vdots & \vdots & \vdots & \vdots \\ h_0(f_{N_f}/s_2) & -h_2(f_{N_f}/s_2) & \cdots & (-1)^{\frac{N}{2}-1} h_{N-1}(f_{N_f}/s_2) \\ -h_1(f_1/s_2) & h_3(f_1/s_2) & \cdots & (-1)^{\frac{N}{2}} h_{N-2}(f_1/s_2) \\ \vdots & \vdots & \vdots & \vdots \\ -h_1(f_{N_f}/s_2) & h_3(f_{N_f}/s_2) & \cdots & (-1)^{\frac{N}{2}} h_{N-2}(f_{N_f}/s_2) \end{bmatrix}_{(N_t+2N_f)\times N}$$

$$\cdot \begin{bmatrix} a_1 \\ a_2 \\ \vdots \\ a_{N-1} \end{bmatrix}_{N\times 1} = \begin{bmatrix} \sqrt{s_1} f(t_1) \\ \vdots \\ \sqrt{s_1} f(t_{N_t}) \\ \sqrt{s_2} F_R(f_1) \\ \vdots \\ \sqrt{s_2} F_R(f_{N_f}) \\ \sqrt{s_2} F_I(f_1) \\ \vdots \\ \sqrt{s_2} F_I(f_{N_f}) \end{bmatrix}_{(N_t+2N_f)\times 1}$$

(8.24)

Therefore, in (8.24) using the early time-domain data from $f(t_1), f(t_2), \ldots, f(t_{N_t})$ and the low frequency-domain data $F(f_1), F(f_2), \ldots, F(f_{N_f})$ the unknown coefficients of

the expansion are obtained by solving a least-squares problem using singular value decomposition [1-3]. Using the obtained unknown coefficients one can then construct function representations to extrapolate both early time and low frequency domain data to late-time and high-frequency domain data.

V. RESULTS

To validate the technique of using only early-time and low-frequency data, which contain mutually complementary information, to simultaneously extrapolate the entire system response in both domains using the orthonormal associate hermite (AH) functions, consider a simple dipole antenna of length $l = 1.0\,\mathrm{m}$ and radius $a = .001\,\mathrm{m}$ loaded with a resistive load of $R = 100\,\Omega$ in free space. The current in the load of this dipole is characterized in the time domain using FDTD and in the frequency domain using MOM, as described in Chapter 5. The number of unknowns used to approximate the current distribution on the antenna for MOM is 63, and the FDTD cell size used to obtain the time-domain results is $\Delta x = \Delta y = \Delta z = \Delta = 1/63\ \mathrm{m}$. The load is positioned at the 48$^{\text{th}}$ segment, which corresponds to the middle of the monopole. One can use any arbitrary excitation as a voltage source at the feed to generate the current in the load, but the excitation used here is a Gaussian source expressed as

$$V_{inc} = e^{-\gamma^2/2} \tag{8.25}$$

where $\gamma = (t - t_0)/\sigma$, t_0 is a delay used to make the pulse rise smoothly from zero for time $t < 0$ to its value at t, and σ represents the standard deviation of the Gaussian

distribution. The Gaussian excitation waveform and its frequency spectrum are shown in Fig. 3-2.

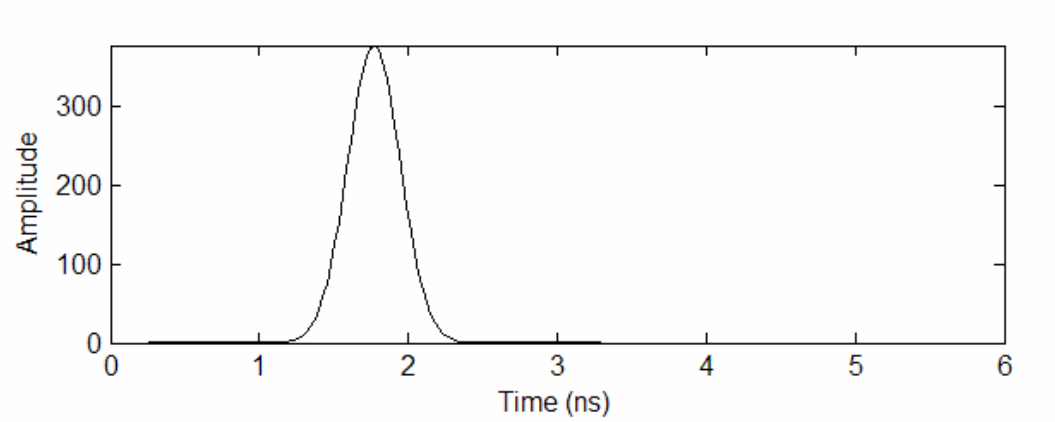

(c) Gaussian excitation waveform in the time domain

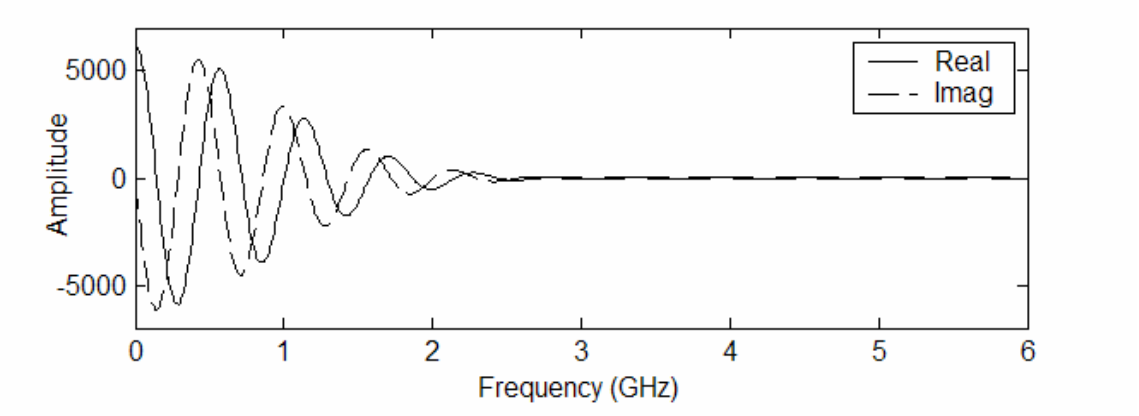

(d) The frequency spectrum of the excitation waveform of (a)

Fig. 3-2. The Gaussian voltage source introduced at the feed point of the thin-wire antenna

To obtain the frequency domain response of the loaded dipole subjected to the above Gaussian pulse, the frequency domain data obtained using the MOM has to be multiplied by the spectrum of the time-domain Gaussian pulse.

The time-domain results shown in Fig. 3-3 are obtained from $t = 0$ to $t = 13.4502\,\text{ns}$ (500 data points) using FDTD, and the frequency-domain results

shown in Fig. 3-4 (a) are obtained from DC to $f = 3.9980\,\text{GHz}$ (2,000 data points) using MOM. The frequency response of the wire antenna in Fig. 3-4 (b) is computed by multiplying the frequency-domain data obtained by MOM with the spectrum of the Gaussian pulse of Fig. 3-2 (b).

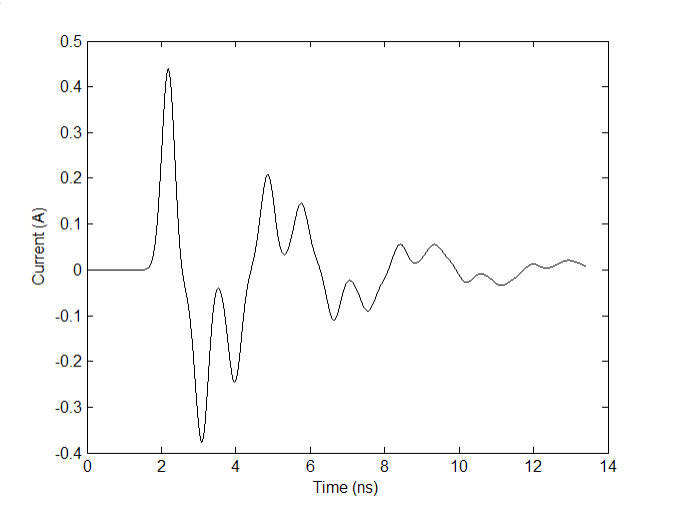

Fig. 3-3. The time-domain data for the current in the load of a dipole antenna of length $l = 1.0\,\text{m}$ and radius $a = .001\,\text{m}$ loaded with a resistive load of $R = 100\,\Omega$ in free space

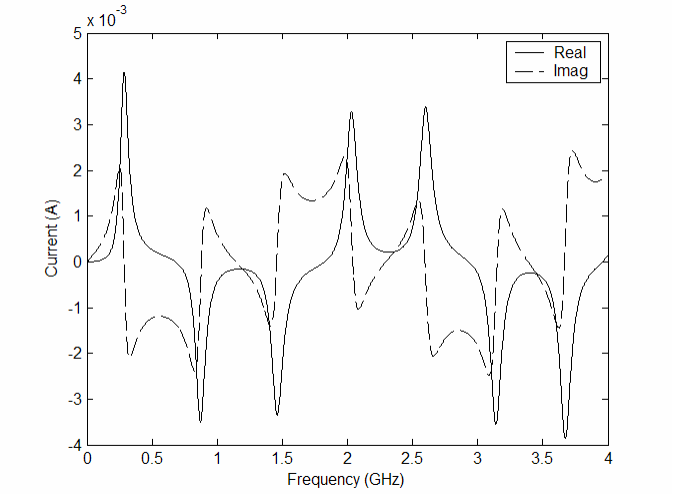

(a) Frequency domain data obtained via MOM

Fig. 3-4. The frequency-domain data for the current in the load of a dipole antenna of length $l = 1.0\,\text{m}$ and radius $a = .001\,\text{m}$ loaded with a resistive load of $R = 100\,\Omega$ in free space (Continued)

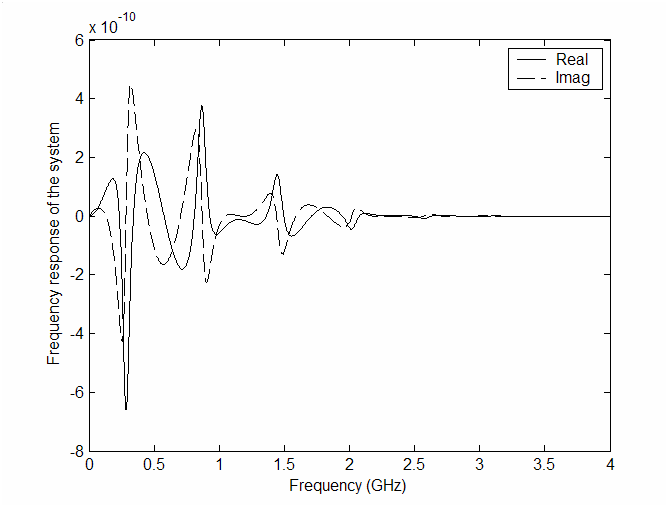

(b) Frequency response of the system

Fig. 3-4. The frequency-domain data for the current in the load of a dipole antenna of length $l = 1.0\,\text{m}$ and radius $a = .001\,\text{m}$ loaded with a resistive load of $R = 100\,\Omega$ in free space

As mentioned earlier, one can extrapolate the time- and frequency-domain data by using sufficient low-frequency $\left(N_f\right)$ and early time-domain data $\left(N_t\right)$, a properly chosen order of expansion *N*, and scale factors s_1 and s_2. For the time being, consider an expansion of order $N = 100$ having scale factors chosen so that the frequency range of the available data is mapped to $\left(-6, 6\right)$. Assuming that only the first 180 data points are available in the time domain $\left(N_t\right)$ and only the first 700 data points are available in the frequency domain $\left(N_f\right)$, the matrix equation given by (8.24), when solved for the unknown coefficients, can be used to extrapolate the time-domain data to $t = 13.4502\,\text{ns}$ (500 data points) and the frequency-domain data to $f = 3.9980\,\text{GHz}$ (2,000 data points), as shown in Fig. 3-5.

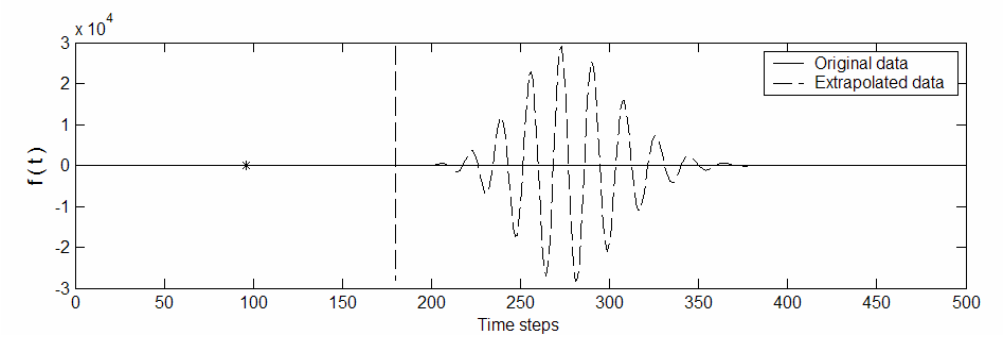

(a) Time-domain response

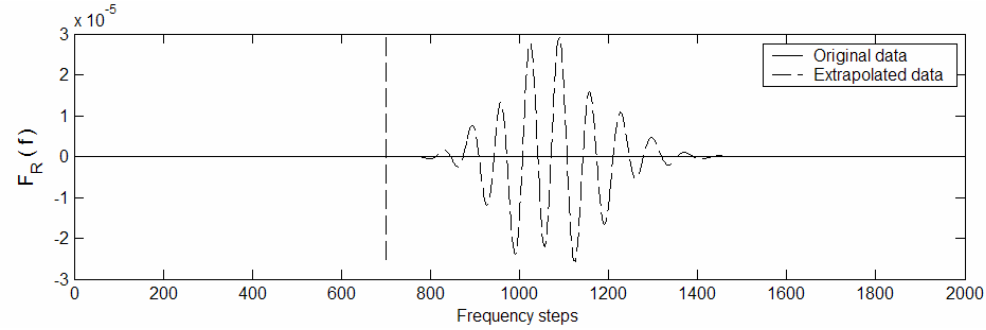

(c) Real part of the frequency response

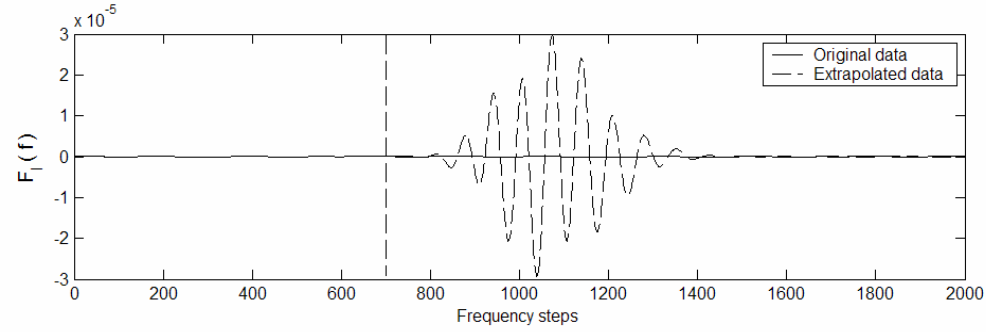

(d) Imaginary part of the frequency response

Fig. 3-5. The original data and the extrapolated data for (a) time-domain, (b) real part of frequency-domain response, (c) imaginary part of frequency-domain response, and (d) the unknown expansion coefficients of the AHF for a resistively loaded dipole of length $l = 1.0\,\mathrm{m}$, $a = .001\,\mathrm{m}$, and $R = 100\,\Omega$ for $N_t = 180$, $N_f = 700$, N =100, and the frequency range of the available data mapped to $(-6, 6)$ (Continued)

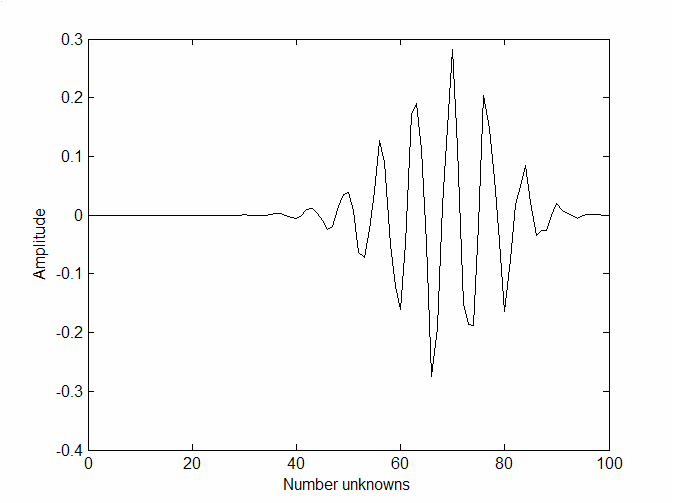

(e) The unknown coefficients

Fig. 3-5. The original data and the extrapolated data for (a) time-domain, (b) real part of frequency-domain response, (c) imaginary part of frequency-domain response, and (d) the unknown expansion coefficients of the AHF for a resistively loaded dipole of length $l = 1.0\,\mathrm{m}$, $a = .001\,\mathrm{m}$, and $R = 100\,\Omega$ for $N_t = 180$, $N_f = 700$, N =100, and the frequency range of the available data mapped to $(-6, 6)$

The time-domain waveform is centered about $t_c = 2.5555(ns)$, which is denoted by an asterisk in Fig. 3-5 (a). The data assumed to be available in both domains is separated from the extrapolated data by vertical dashed lines. The results are incorrect and show significant/large late time and high frequency oscillations, indicating insufficient amount of support being provided by the AH functions to the time and frequency domain data. This can be corrected by increasing the scale factor so that the frequency range of the available data is mapped to $(-13, 13)$. Given the same time-domain and frequency-domain data as before, the solution of the matrix equation given by (8.24) for the unknown coefficients yields the results shown in Fig. 3-6.

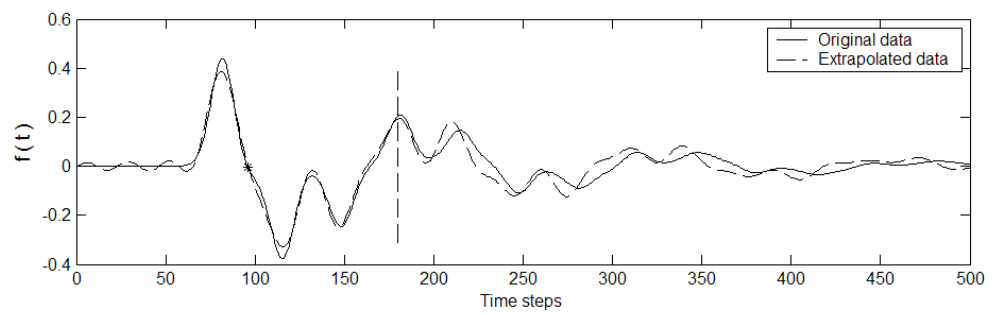

(a) Time-domain response

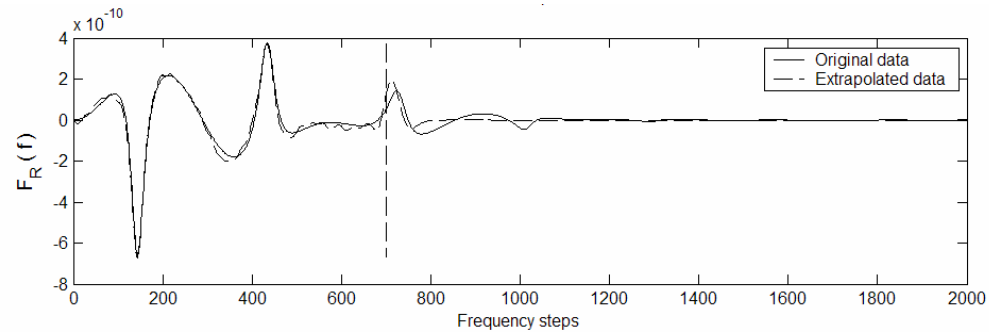

(b) Real part of the frequency response

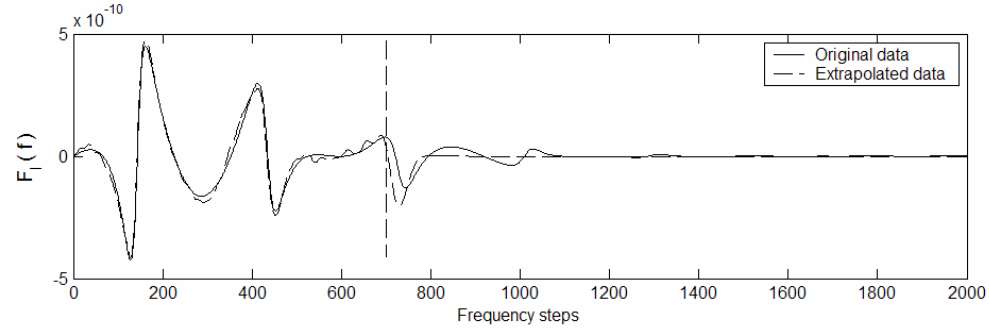

(c) Imaginary part of the frequency response

Fig. 3-6. The original data and the extrapolated data for (a) time-domain, (b) real part of frequency-domain response, (c) imaginary part of frequency-domain response and (d) the unknown expansion coefficients of the AHF for a resistively loaded dipole of length $l = 1.0\,\mathrm{m}$, $a = .001\,\mathrm{m}$, and $R = 100\,\Omega$ for $N_t = 180$, $N_f = 700$, N =100, and the frequency range of the available data mapped to $(-13, 13)$ (Continued)

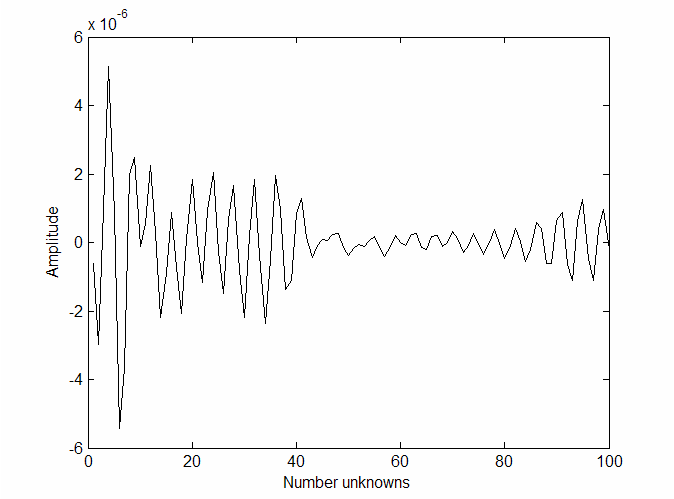

(d) The unknown coefficients

Fig. 3-6. The original data and the extrapolated data for (a) time-domain, (b) real part of frequency-domain response, (c) imaginary part of frequency-domain response and (d) the unknown expansion coefficients of the AHF for a resistively loaded dipole of length $l = 1.0\,\mathrm{m}$, $a = .001\,\mathrm{m}$, and $R = 100\,\Omega$ for $N_t = 180$, $N_f = 700$, N =100, and the frequency range of the available data mapped to $(-13, 13)$

The time-domain waveform is again centered about $t_c = 2.5555(ns)$ and denoted by an asterisk in Fig. 3-6 (a). These results are much better than the results in Fig. 3-5 but still do not agree with the original data even in the range of the available data. The amplitude of the plot of unknown coefficients in Fig. 3-6 (d) tends to increase for higher orders of expansion, indicating that an insufficient amount of either time- or frequency-domain data is considered. Hence, increasing the number of available data points in the frequency domain (N_f) from 700 to 1000 data points and using the same order of expansion, scale factor, and number of time-domain data points as before, much more agreeable results are obtained, as shown in Fig. 3-7.

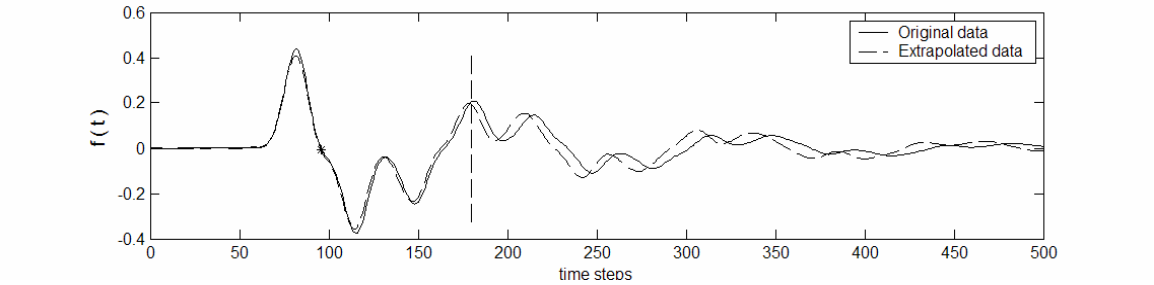

(a) Time-domain response

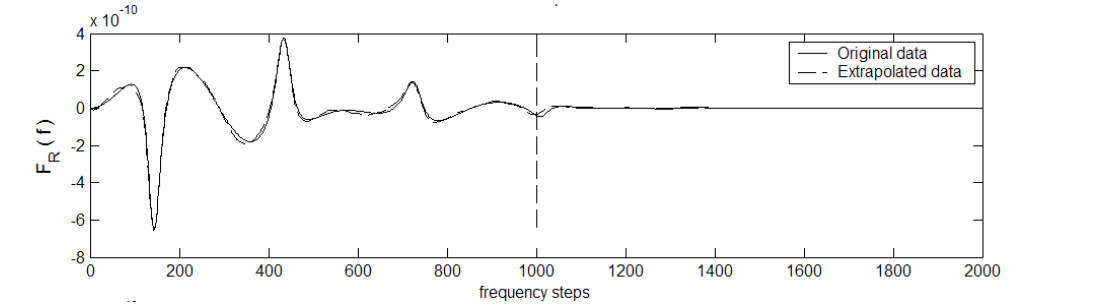

(b) Real part of the frequency response

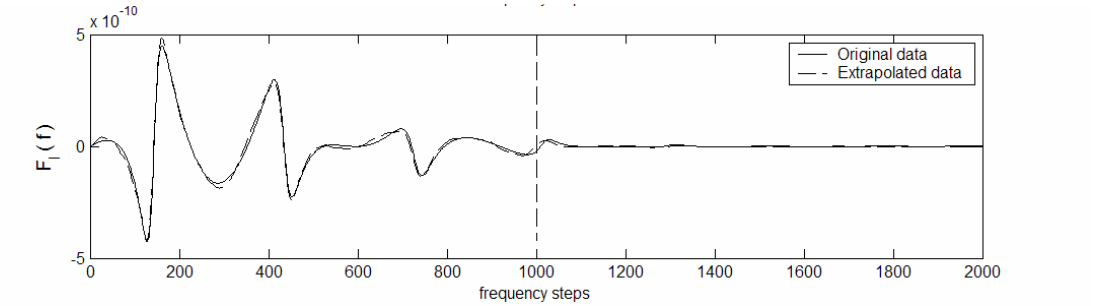

(c) Imaginary part of the frequency response

Fig. 3-7. The original data and the extrapolated data for (a) time-domain, (b) real part of frequency-domain response, (c) imaginary part of frequency-domain response, and (d) the unknown expansion coefficients of the AHF for a resistively loaded dipole of length $l = 1.0\,\mathrm{m}$, $a = .001\,\mathrm{m}$, and $R = 100\,\Omega$ for $N_t = 180$, $N_f = 1000$, N =100, and the frequency range of the available data mapped to $(-13, 13)$ (Continued)

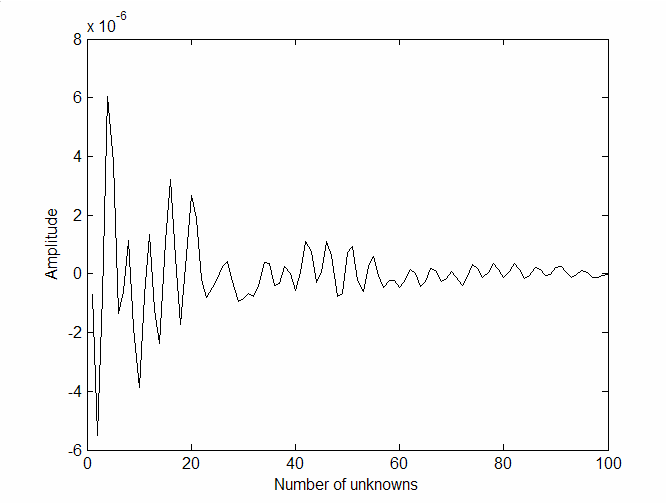

(d) The unknown coefficients

Fig. 3-7. The original data and the extrapolated data for (a) time-domain, (b) real part of frequency-domain response, (c) imaginary part of frequency-domain response, and (d) the unknown expansion coefficients of the AHF for a resistively loaded dipole of length $l = 1.0\,\mathrm{m}$, $a = .001\,\mathrm{m}$, and $R = 100\,\Omega$ for $N_t = 180$, $N_f = 1000$, N =100, and the frequency range of the available data mapped to $(-13, 13)$

The time-domain waveform is centered about $t_c = 2.5555(ns)$, denoted by an asterisk in Fig. 3-7 (a), and the data assumed to be available in both domains is separated from the extrapolated data by vertical dashed lines. The plot of the unknown coefficients shows the coefficients dying out for higher orders of expansion, which is expected [1-3]. From Fig. 3-7 one can say that the extrapolated data is agreeable in comparison to the original data. The slight mismatch between the original data and extrapolated data in Fig. 3-5 (a) for later time steps can be attributed to grid dispersion errors in FDTD, which are explained in Chapters 2 and 5. Hence, for a given time-bandwidth product of 9.6207, one is able to extrapolate to a time-bandwidth product of 53.6662.

The CPU times taken to compute the assumed available time-domain and frequency-domain data on a 2.08 GHz processor with 2.0 GB of RAM are 13.47 and

23.07 minutes, respectively, yielding a total time of 36.54 minutes. If one were to compute the entire range of time-domain and frequency-domain data without using extrapolation techniques, it would take 37.30 minutes for time-domain calculations and 45.26 minutes for frequency-domain calculations. The amount of CPU time saved for the simple case of a loaded dipole antenna is 46.02 minutes. This CPU time savings becomes even more significant when calculating the electromagnetic responses of complex cavity structures in both domains, a process that is normally very computationally intensive and time-consuming. It is clear that the extrapolation techniques can significantly reduce the amount of CPU time used.

Now consider a simple dipole antenna of length $l = 2.0\,\mathrm{m}$ and radius $a = .005\,\mathrm{m}$ in free space. The current at the feed point of this dipole is characterized in the time domain using FDTD and in the frequency domain using MOM, as described in Chapter 5. The number of unknowns used to approximate the current distribution on the antenna for MOM is 601, and the FDTD cell size used to obtain the time-domain results is $\Delta x = \Delta y = \Delta z = \Delta = 0.0392\ \mathrm{m}$. The time-domain results are obtained from $t = 0$ to $t = 19.6214\,\mathrm{ns}$ (300 data points) using FDTD, and the frequency-domain results shown in Fig. 3-8 (a) are obtained from DC to $f = 4.0\,\mathrm{GHz}$ (2,000 data points) using MOM. The frequency response of the wire antenna is again obtained by multiplying the frequency-domain data obtained by MOM with the spectrum of the incident voltage waveform used in the FDTD code. Assuming that only the first 100 data points are available in the time domain and only the first 650 data points are available in frequency domain, one can solve the matrix equation given by (8.24) for the unknown coefficients and successfully extrapolate the time-domain data to $t = 19.6214\,\mathrm{ns}$ (300 data points) and the frequency-

domain data to $f = 4.0\,\text{GHz}$ (2,000 data points), as shown in Fig. 3-8. The order of the expansion is chosen to be $N = 90$ and the plot of the unknown coefficients of (9.24) is as shown in Fig. 3-8 (d). The time-domain waveform is centered about $t_c = 4.9054(ns)$, which is denoted by an asterisk in Fig. 3-8 (a). The choice of l_2 was made so that the frequency range of the available data is mapped to $(-12, 12)$.

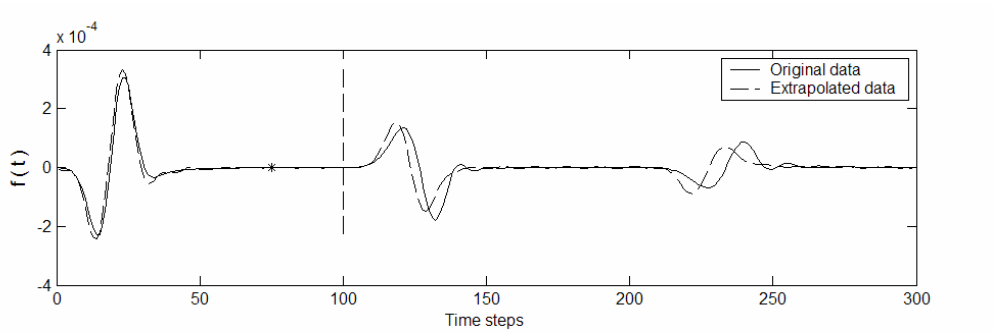

(a) Time-domain response

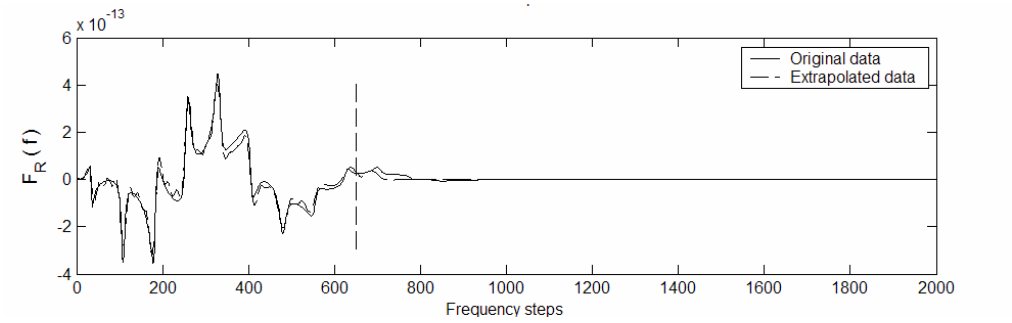

(b) Real part of the frequency response

Fig. 3-8. The original data and the extrapolated data for (a) time-domain, (b) real part of frequency-domain response, (c) imaginary part of frequency-domain response, and (d) the unknown expansion coefficients of the AHF for the current at the feed point of a dipole $l = 2.0\,\text{m}$ and $a = .005\,\text{m}$ for $N_t = 100$, $N_f = 650$, N =90, and the frequency range of the available data mapped to $(-12, 12)$ (Continued)

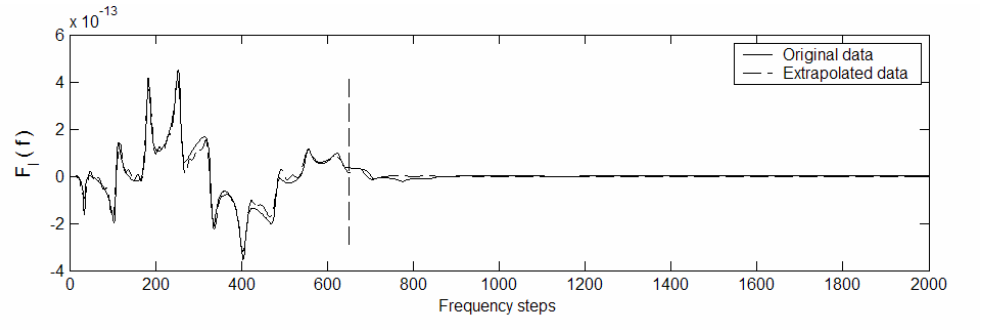

(c) Imaginary part of the frequency response

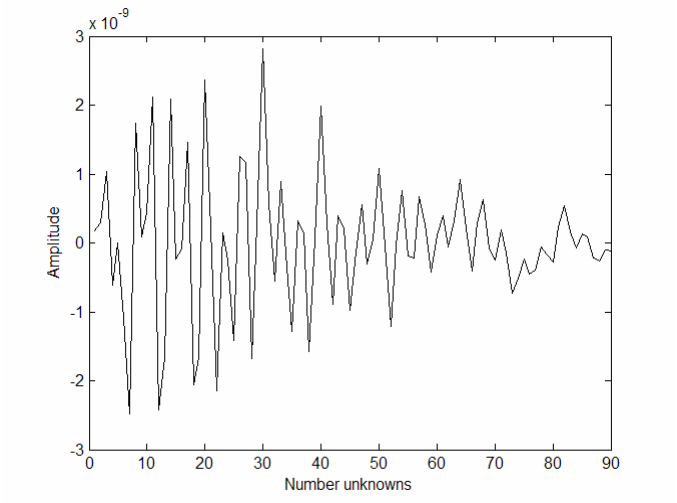

(d) The unknown coefficients

Fig. 3-8. The original data and the extrapolated data for (a) time-domain, (b) real part of frequency-domain response, (c) imaginary part of frequency-domain response, and (d) the unknown expansion coefficients of the AHF for the current at the feed point of a dipole $l = 2.0\,\mathrm{m}$ and $a = .005\,\mathrm{m}$ for $N_t = 100$, $N_f = 650$, N =90, and the frequency range of the available data mapped to $(-12, 12)$

In Fig. 3-8 the data assumed to be available in both domains is separated from the extrapolated data by vertical dashed lines. The extrapolated data is agreeable in comparison to the original data with a slight mismatch between the original data and extrapolated data for later time steps. Hence, for a given time-bandwidth product of 8.5026, one is able to extrapolate to a time-bandwidth product of 78.4857.

Lastly, consider another case of a simple dipole antenna of length $l = 1.0\,\mathrm{m}$ and radius $a = .001\,\mathrm{m}$ in free space. The current at the feed point of this dipole is again characterized in the time domain using FDTD and in the frequency domain using MOM, as described in Chapter 5. The number of unknowns used to approximate the current distribution on the antenna for MOM is 63, and the FDTD cell size used to obtain the time-domain results is $\Delta x = \Delta y = \Delta z = \Delta = 1/63$ m. The time-domain results are obtained from $t = 0$ to $t = 19.8550\,\mathrm{ns}$ (750 data points) using FDTD, and the frequency-domain results shown in Fig. 3-9 (a) are obtained from DC to $f = 4.0\,\mathrm{GHz}$ (2,000 data points) using MOM. The frequency response of the wire antenna is again obtained by multiplying the frequency-domain data obtained by MOM with the spectrum of the incident voltage waveform used in the FDTD code. Assuming that only the first 190 data points are available in the time domain and only the first 900 data points are available in frequency domain, one can solve the matrix equation given by (8.24) for the unknown coefficients and successfully extrapolate the time-domain data to $t = 19.8550\,\mathrm{ns}$ (750 data points) and the frequency-domain data to $f = 4.0\,\mathrm{GHz}$ (2,000 data points), as shown in Fig. 3-9. The order of the expansion is chosen to be N = 100 and the plot of the unknown coefficients of (9.24) is as shown in Fig. 3-8 (d). The time-domain waveform is centered about $t_c = 2.6473(ns)$, which is denoted by an asterisk in Fig. 3-9 (a). The choice of l_2 was made so that the frequency range of the available data is mapped to $(-13, 13)$.

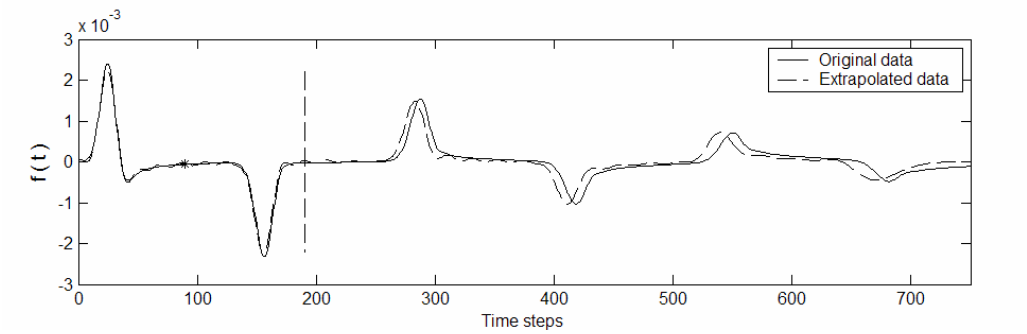

(a) Time-domain response

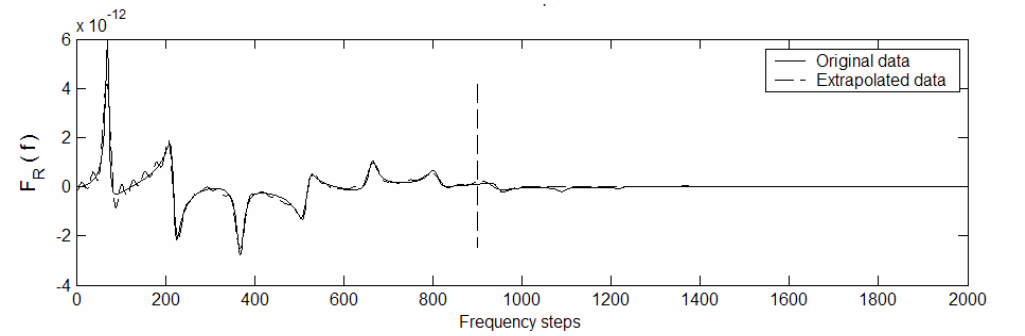

(b) Real part of the frequency response

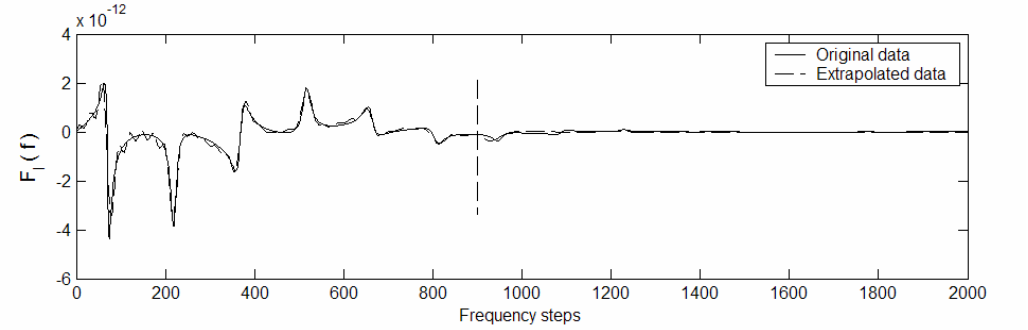

(c) Imaginary part of the frequency response

Fig. 3-9. The original data and the extrapolated data for (a) time-domain, (b) real part of frequency-domain response, (c) imaginary part of frequency-domain response, and (d) the unknown expansion coefficients of the AHF for the current at the feed point of a dipole $l = 1.0\,\mathrm{m}$ and $a = .001\,\mathrm{m}$ for $N_t = 190$, $N_f = 900$, N =100, and the frequency range of the available data mapped to $(-13, 13)$ (Continued)

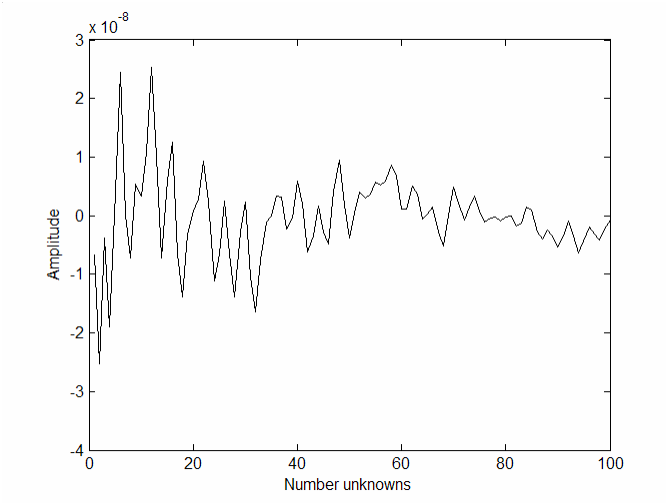

(d) The unknown coefficients

Fig. 3-9. The original data and the extrapolated data for (a) time-domain, (b) real part of frequency-domain response, (c) imaginary part of frequency-domain response, and (d) the unknown expansion coefficients of the AHF for the current at the feed point of a dipole $l = 1.0\,\text{m}$ and $a = .001\,\text{m}$ for $N_t = 190$, $N_f = 900$, N =100, and the frequency range of the available data mapped to $(-13, 13)$

The data assumed to be available in both domains is separated from the extrapolated data by vertical dashed lines in Fig. 3-9. The extrapolated data is agreeable in comparison to the original data with a slight mismatch between the original data and extrapolated data for later time steps. Hence, for a given time-bandwidth product of 9.0539, one is able to extrapolate to a time-bandwidth product of 79.4200.

VI. SUMMARY

In this chapter, simultaneous extrapolation technique for both time-domain and frequency-domain data using associate hermite functions is elucidated. The theoretical formulation is explained in detail, and results are clearly illustrated. The results for a loaded dipole show good agreement between the original data and the extrapolated data, proving that these techniques work. This technique requires significantly less time and

computer memory than the conventional approach involving use of either FDTD or MOM tools separately.

REFERENCES

[1] Rao, M. M., Sarkar, T. K., Anjali, T. and Adve, R. S., "Simultaneous Extrapolation in Time and Frequency Domains Using Hermite Expansions," IEEE Transactions on Antennas & Propagation, Vol. 47, No. 6, pp. 1109-1115, Jun. 1999.

[2] Rao, M. M., Sarkar, T. K., Adve, R. S., Anjali, T. and Callejon, J. F., "Extrapolation of Electromagnetic Responses from Conducting Objects in Time and Frequency Domains," IEEE Transactions on Microwave Theory & Techniques, Vol.47, No. 10, pp. 1964-1974, Oct. 1999.

[3] Tapan K Sharkar, Jinhwan Koh, Wonwoo Lee, and Magdalena Salazar Palma, “Analysis of electromagnetic systems irradiated by ultra-short ultra-wideband pulse”, Measurement Science and Technology, Publication 21, pp. 1757-1768, Oct. 2001.